AD-A134 595 ICE ACTION ON PAIRS OF CYLINDRICAL AND CONICAL STRUCTURES(U) COLD REGIONS RESEARCH AND ENGINEERING LAB HANOVER NH K KATO ET AL. SEP 83 CRREL-83-25 1/1

UNCLASSIFIED F/G 8/12 NL

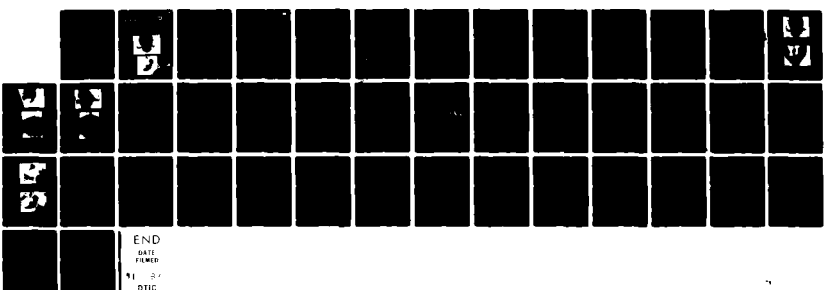

END

DATE FILMED

DTIC

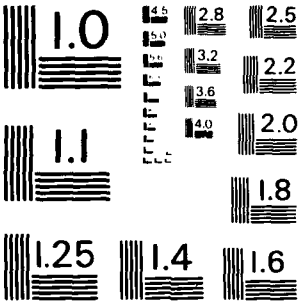

(12)

CRREL REPORT 83-25

AD-A134 595

US Army Corps of Engineers
Cold Regions Research & Engineering Laboratory

Ice action on pairs of cylindrical and conical structures

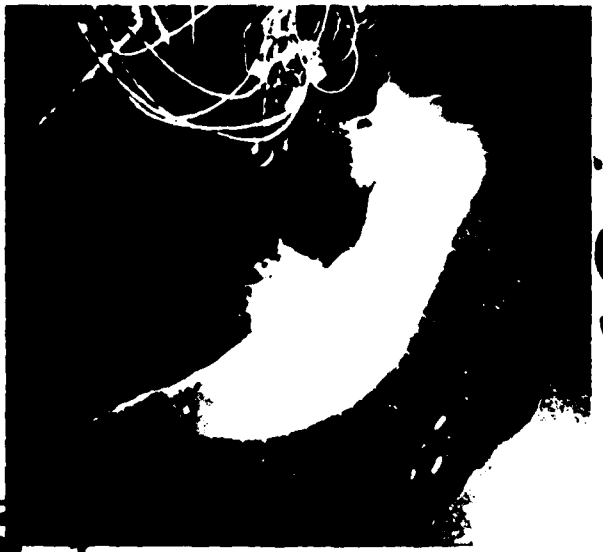

Cover: Pairs of cylindrical (top) and conical (bottom) structures being pushed through a stationary ice cover.

CRREL Report 83-25

September 1983

Ice action on pairs of cylindrical and conical structures

K. Kato and D.S. Sodhi

Prepared for
OFFICE OF THE CHIEF OF ENGINEERS

Unclassified

SECURITY CLASSIFICATION OF THIS PAGE (When Data Entered)

REPORT DOCUMENTATION PAGE	READ INSTRUCTIONS BEFORE COMPLETING FORM
1. REPORT NUMBER CRREL Report 83-25	2. GOVT ACCESSION NO. AD-A134 595
3. RECIPIENT'S CATALOG NUMBER	
4. TITLE (and Subtitle) ICE ACTION ON PAIRS OF CYLINDRICAL AND CONICAL STRUCTURES	5. TYPE OF REPORT & PERIOD COVERED
	6. PERFORMING ORG. REPORT NUMBER
7. AUTHOR(s) K. Kato and D.S. Sodhi	8. CONTRACT OR GRANT NUMBER(s)
9. PERFORMING ORGANIZATION NAME AND ADDRESS U.S. Army Cold Regions Research and Engineering Laboratory Hanover, New Hampshire 03755	10. PROGRAM ELEMENT, PROJECT, TASK AREA & WORK UNIT NUMBERS CWIS 31723
11. CONTROLLING OFFICE NAME AND ADDRESS Office of the Chief of Engineers Washington, D.C. 20314	12. REPORT DATE September 1983
	13. NUMBER OF PAGES 42
14. MONITORING AGENCY NAME & ADDRESS(if different from Controlling Office)	15. SECURITY CLASS. (of this report) Unclassified
	15a. DECLASSIFICATION/DOWNGRADING SCHEDULE

16. DISTRIBUTION STATEMENT (of this Report)

Approved for public release; distribution unlimited.

17. DISTRIBUTION STATEMENT (of the abstract entered in Block 20, if different from Report)

18. SUPPLEMENTARY NOTES

19. KEY WORDS (Continue on reverse side if necessary and identify by block number)

Bridges	Ice forces
Bridge piers	Interactions
Conical test structures	Interactions of two structures
Cylindrical test structures	Pier spacing
Ice	

20. ABSTRACT (Continue on reverse side if necessary and identify by block number)

Ice action on two cylindrical and conical structures, located side by side, has been investigated in a small-scale experimental study to determine the interference effects on the ice forces generated during ice-structure interaction. The proximity of the two structures changes the mode of ice failure, the magnitude and direction of ice forces on the individual structure, and the dominant frequency of ice force variations. Interference effects were determined by comparing the experimental results of tests at different structure spacings.

DD FORM 1 JAN 73 1473 EDITION OF 1 NOV 65 IS OBSOLETE

Unclassified

SECURITY CLASSIFICATION OF THIS PAGE (When Data Entered)

PREFACE

This report was prepared by Kazuyuki Kato, Research Engineer, Ishikawajima-Harima Heavy Industries, Tokyo, Japan, and Dr. Devinder S. Sodhi, Research Hydraulic Engineer, Ice Engineering Research Branch, Experimental Engineering Division, U.S. Army Cold Regions Research and Engineering Laboratory. Funding for this project was provided by Civil Works Program, *Ice Engineering*, CWIS 31723, *Model Studies and Ice Effects on Structures.*

F.D. Haynes and W.B. Tucker III, both of CRREL, provided technical review. K. Kato is deeply grateful to all CRREL personnel—particularly the Ice Engineering Research Branch—for the hospitality extended to him during his stay. Both authors express their appreciation for the help and support received during the experiments from A.E. Lozeau, S.L. DenHartog, C.L. Ackerman, C.I. Schelewa, C.R. Martinson, F.D. Haynes, Dr. J.C. Tatinclaux and the personnel of CRREL's Technical Services Division.

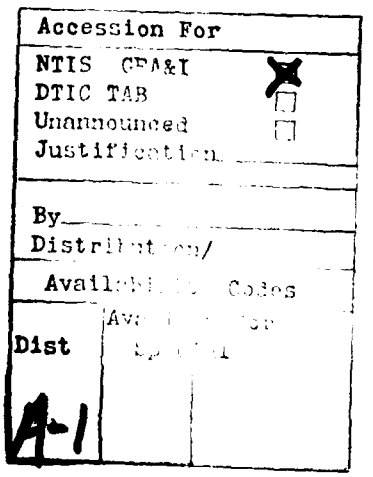

CONTENTS

	Page
Abstract	i
Preface	ii
Nomenclature	v
Introduction	1
Experimental setup and procedure	1
Results and discussion	3
Cylindrical structures	3
Conical structures	18
Conclusions	21
Literature cited	22
Appendix A: Relationship between flexural strength and in-situ unconfined compressive strength	25
Appendix B: Test data	27

ILLUSTRATIONS

Figure

1. Experimental setup for cylindrical structures	2
2. Compressive strengths of columnar ice	3
3. Crushing failure	4
4. Tracks made by structures	5
5. Lateral cracks in the ice between the structures	6
6. Ice force records	7
7. Typical longitudinal and transverse ice force records	8
8. Ice forces versus aspect ratio	9
9. Normalized maximum forces versus ratio of center-to-center distance to structure diameter	10
10. Normalized mean forces versus ratio of center-to-center distance to structure diameter	10
11. Ratio of maximum transverse and longitudinal forces versus ratio of center-to-center distance to structure diameter	11
12. Resultant force direction θ versus S for the 152-mm-diameter structure	11
13. Autospectra of ice force records	12
14. Ice-induced vibration frequency versus velocity	13
15. Ice-induced vibration frequencies versus ice thickness	14
16. Combined plot of ice-induced vibration frequency versus velocity for test series 500 and 900	15
17. Ice-induced vibration frequencies versus ratio of relative velocity to thickness of ice sheet for different structure diameters	16
18. Coefficient C versus structure diameter and aspect ratio	16
19. Normalized buckling loads versus ratio of structure diameter to characteristic length of ice sheet	17
20. Normalized buckling load against two structures versus ratio of equivalent width of two structures to characteristic length	17

Figure		Page
21.	Experimental setup for conical structures	18
22.	Failure of an ice sheet against two conical structures	19
23.	Ice force records for failure of ice against two conical structures	20
24.	Normalized maximum ice force versus ice velocity	20
25.	Normalized initial peak force versus ice velocity	21
26.	Ratio of initial peak ice force to theoretical ice force versus ratio of center-to-center distance between structures to characteristic length	21

NOMENCLATURE

d diameter of cylindrical structures (mm)

f frequency of ice force fluctuations (Hz)

h thickness of ice sheet (mm)

k stiffness of structures (N/m)

v relative velocity of the structures with respect to the ice sheet (mm/s)

B_e equivalent width of two structures in case of common buckling failure, $B_e = d + S$ (mm)

C coefficient defined in eq 7

F_b buckling load (N)

F_e buckling load in case of common buckling failure—summation of buckling load on two structures (N)

F_i initial peak force on conical structure (N)

F_{max} maximum force on conical structure (N)

F_r theoretical ice force on conical structure (N)

F_x longitudinal ice force in the direction of the structure movement—see Figure 2 (N)

F_{xmax} maximum of F_x during a test (N)

F_{xmean} average of F_x during a test (N)

F_y transverse ice force, perpendicular to structure movement—see Figure 2 (N)

F_{ymax} maximum of F_y during a test (N)

F_z vertical ice force (N)

K specific weight of water—foundation modulus (N/m^3)

L characteristic length of a floating ice sheet (mm)

S center-to-center distance between two structures (mm)

$\dot{\epsilon}$ strain rate estimated from eq 1 (s^{-1})

θ direction of resultant force as defined in Figure 2 (°)

σ_c confined compressive strength of columnar ice sheet—see Figure 3 (N/m^2)

σ_f flexural strength of ice (kPa)

σ_u unconfined compressive strength of columnar ice sheet as determined from in situ tests—see Figure 3 (kPa)

ICE ACTION ON PAIRS OF CYLINDRICAL AND CONICAL STRUCTURES

K. Kato and D.S. Sodhi

INTRODUCTION

This experimental study investigates the ice forces generated during an ice action on two structures that are situated side by side. This study is motivated by the need to understand the interaction with moving ice of two or more legs of an offshore structure, such as an oil drilling platform. We expect ice actions and the resulting ice forces to be different from those on a single, isolated structure. If the distance between the structures is small, it is possible that the failure of ice around one structure may affect the ice failure around the other structure, and this interaction may influence the ice forces and the vibrations felt by both structures. On the other hand, if the distance between the structures is large, the ice action on one structure may be independent of the other. Since the mode of ice failure depends upon the aspect ratio (ratio of structure width to ice thickness), it is possible for closely spaced structures to act as one structure of increased width and to produce an entirely different mode of failure than the one they would have produced had they interacted with the ice independently.

We observed the mode of ice failure and measured the ice forces when pairs of structures were pushed through an ice sheet. The parameters that were changed during the experimental program were the diameter of the structures, the distance between them and their relative velocity with respect to the ice. The structure shapes used were cylindrical and conical. We attempted to maintain the thickness of the ice sheet within a narrow range. The ice properties were measured intermittently during the experiments, and these were used to normalize the ice forces. The results are presented in terms of maximum and mean force levels. We also investigated the dependence of the dominant frequency of ice force variations on relative velocity, ice thickness and other parameters.

EXPERIMENTAL SETUP AND PROCEDURE

We conducted the experiments by moving the model structures through an ice sheet as shown schematically in Figure 1 (see Fig. 22 for schematic of conical structures setup). In earlier experiments (Haynes et al. 1983), we pushed ice sheets against fixed model structures to study this interaction and to measure the ice forces. In this study, the model structures were mounted on cantilever beams that were held in frames mounted on the lower beam of the carriage in the CRREL test basin. The distance between the structures could be easily changed. The forces were measured by monitoring the response of strain gauges installed on the cantilever beams. The natural frequency of the free vibration of the force-measuring beam was determined to be in the range of 70 to 80 Hz. The amplified data from the strain gauge circuits were filtered with a 10-Hz low pass filter, which had a fall-off rate of −40 dB/decade. On each structure, the forces in three directions could be monitored: F_x, the force component parallel to the structure movement; F_y, the force component perpendicular to the structure movement; and F_z, the vertical force component. The positive directions of all force components are defined in Figure 1.

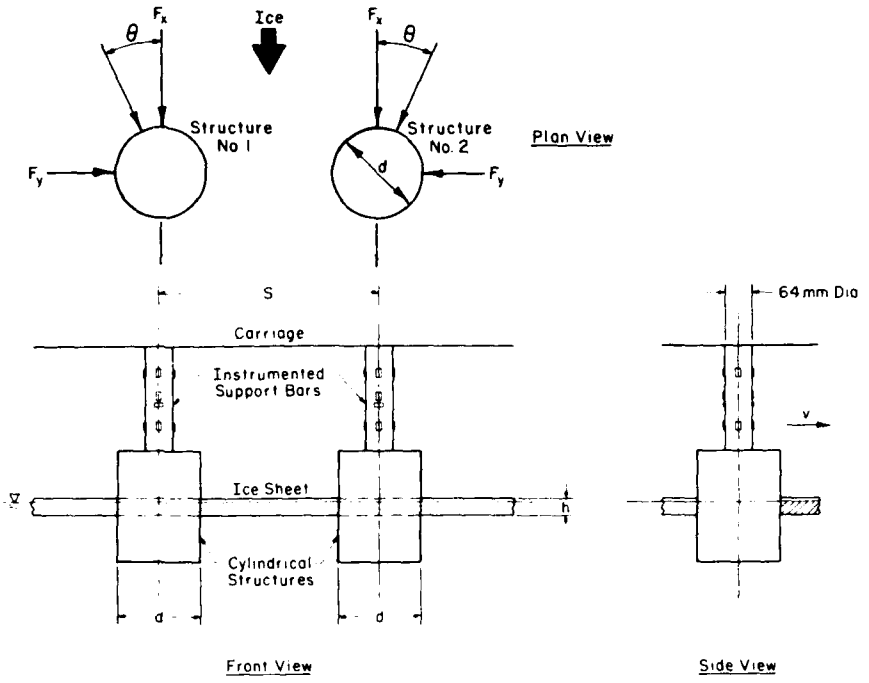

Figure 1. Experimental setup for cylindrical structures (plan view shows force components).

These forces were recorded in both digital and analog forms. The scan interval for the digital data acquisition was 10 ms.

For a particular distance between the pair of structures, tests were performed at four different velocities. A set of four tests is called a test series, and after each test series, the distance between structures was changed. Three to four test series were conducted using one ice sheet.

We tested two different structure shapes—cylindrical and conical. The diameters of the vertical cylindrical structures were 64 mm (2.5 in.), 152 mm (6 in.) and 305 mm (12 in.), and they were made of wood with a skin of smooth aluminum sheeting. The conical structures had a slope of 45° from the horizontal, and their base diameter and height were 540 mm (21.3 in.) and 190 mm (7.5 in.) respectively. One of these was made of plastic and the other was made of wood with an aluminum skin. The surface of the plastic structure appeared to be rougher than the one with the aluminum skin.

The ice sheets were grown by seeding and freezing a 0.95% urea-in-water solution at an ambient temperature of −12°C. The resulting ice sheet had three layers: a thin seed layer at the top, a fine-grained transition layer (about 20% of thickness) and a coarse-grained bottom layer (about 80% of thickness). The texture throughout was columnar. Before each test series, the characteristic length L, flexural strength σ_f and in situ uniaxial compressive strength σ_u of the ice sheet were measured by conducting three different types of tests. We determined the characteristic length of the floating ice sheet by placing dead weights on it in discrete increments and then monitoring its deflection. This procedure is described in detail by Sodhi et al. (1982b). We determined the flexural strength of the ice by pushing down cantilever beams until they failed and computing the flexural strength from the failure load. We conducted the unconfined compressive strength test on weak, laboratory-grown ice in situ by compressing a cantilever beam (Kato et al. 1982). Since this test was not conducted for some test series, we estimated it using a relationship developed between the bending and uniaxial compressive strengths through regression analysis (Appendix A).

It should be noted that the model ice grown in the test basin had a columnar texture, and that the compressive strength of columnar ice is known to

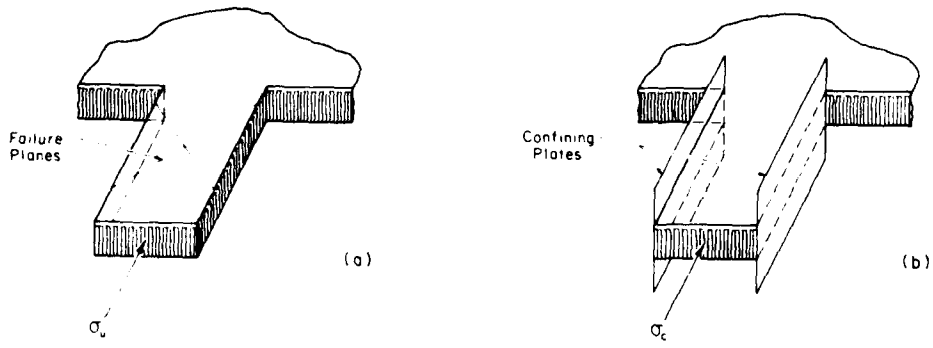

Figure 2. Compressive strengths of columnar ice; a-unconfined; b-confined.

have different values for different crystallographic orientations and different values depending on whether the material is confined or not (Ralston 1978, Frederking 1977). The unconfined and confined compressive strengths of columnar ice are defined by σ_u and σ_c as shown in Figure 2. The significant difference between the unconfined and confined compressive strength tests is the way the ice fails during each test. In the case of an unconfined compressive strength test, the failure takes place along vertical planes resulting in sliding failure. During the confined compressive strength tests, the material is confined laterally to make it move vertically up or down and the failure results in either pulverization of the ice or shearing along inclined planes that cut the vertical columnar crystals. Thus the confined compressive strength is generally higher than the unconfined compressive strength. Since the confined compressive strength σ_c was not measured, it is assumed to be a multiple of confined compressive strength σ_u. This point will be discussed later during the analysis of ice force data on a single, isolated structure.

RESULTS AND DISCUSSION

The results of experiments on cylindrical and conical structures will be presented separately as the ice action on these structures is quite different.

Cylindrical structures

General observations

We identified the failure modes primarily by observation but also by examining the force records for each test. These are summarized in Table B1 along with the conditions for each test.

Basically, we observed three different failure modes during the experiments: continuous crushing, buckling and bending. We sometimes saw a failure mode change during a test, especially from continuous crushing to buckling. We also observed that the different modes of failure took place around each structure in the same test, for example, continuous crushing on one and buckling on the other. When the structures were placed close to each other, the ice sheet buckled in a failure zone common to both structures.

Quite distinguishable from the continuous crushing and buckling modes of failure was bending failure that sometimes took place unexpectedly when the ice sheet was thin and warm. The ice sheet would bend downward and a small amount of flooding could be seen in front of the structure. We also observed a large plastic deformation after the tests with bending failure. Since the force level for this mode of failure was small, the results of these tests are not discussed.

Figure 3 shows photographs of the tests during which continuous crushing took place. The tracks made by the structures in the ice are shown in Figures 4. When the structures were placed relatively close, only one track of the width equal to the combined width of the structures was observed (Fig. 4a). When the structures were located far apart, two tracks of the same width as the diameter of each structure were observed (Fig. 4b). The ice left between the tracks had lateral cracks as shown in Figure 5.

Examples of the force records are given in Figures 6 and 7. We observed that the ice velocity was an important factor in determining the mode of failure. For instance, the ice would buckle against the structure for a particular setup at low velocity and fail in crushing at a higher velocity.

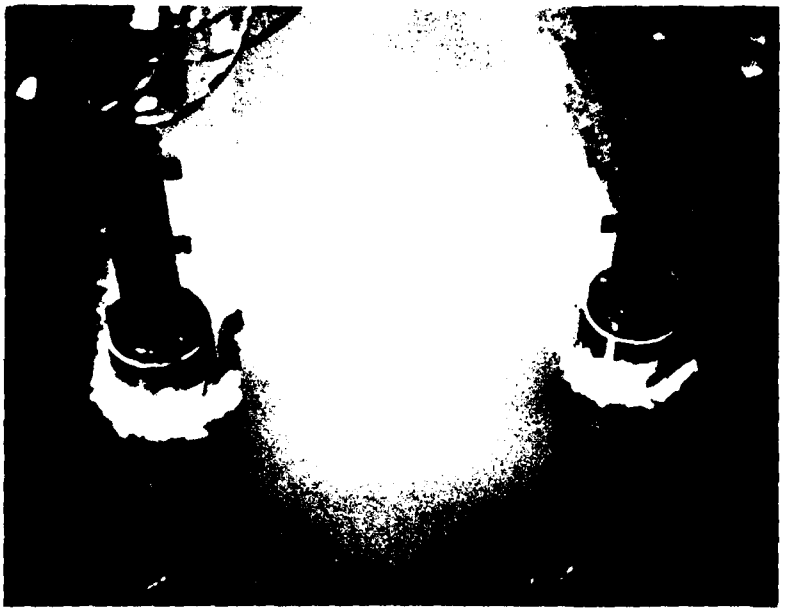

a. Test 142, S = 608 mm.

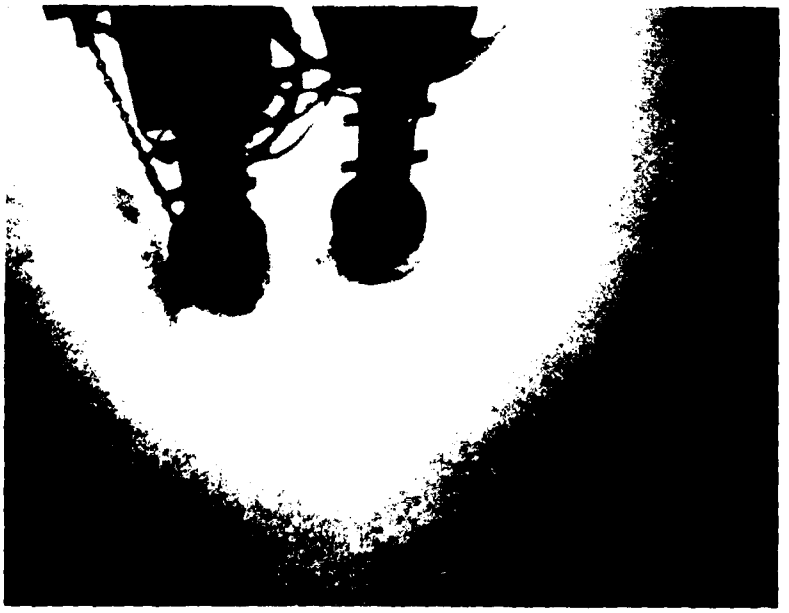

b. Test 122, S = 401 mm.

Figure 3. Crushing failure.

a. S = *401 mm.*

b. S = *608 mm.*

Figure 4. Tracks made by structures.

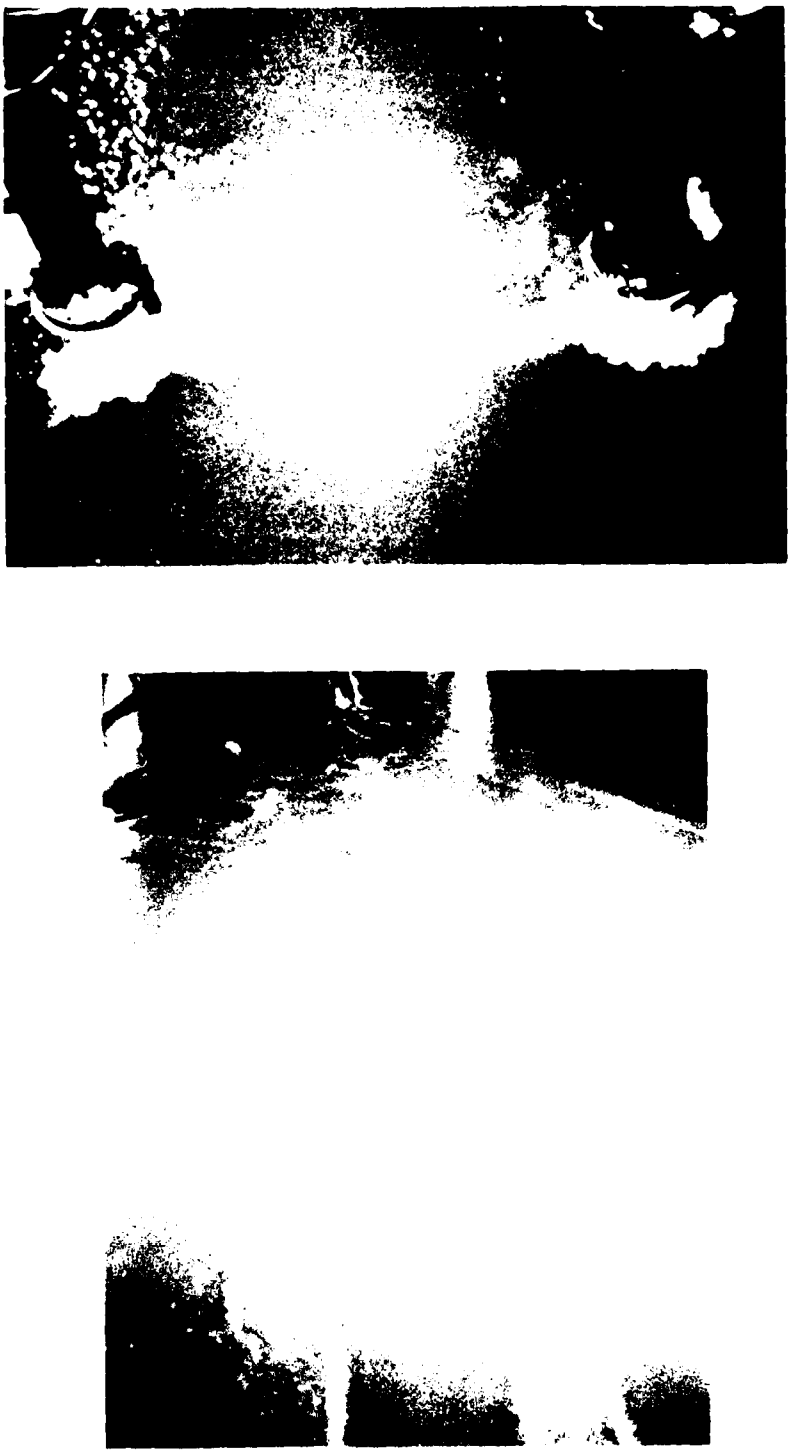

Figure 5. Lateral cracks in the ice between the structures.

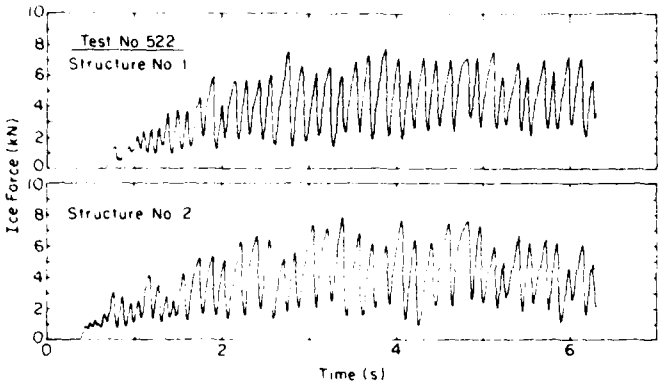

a. Test 522, continuous crushing around both structures.

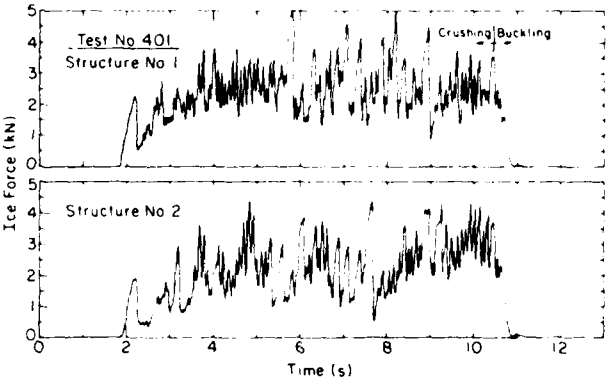

b. Test 401, transition from crushing to buckling across both structures.

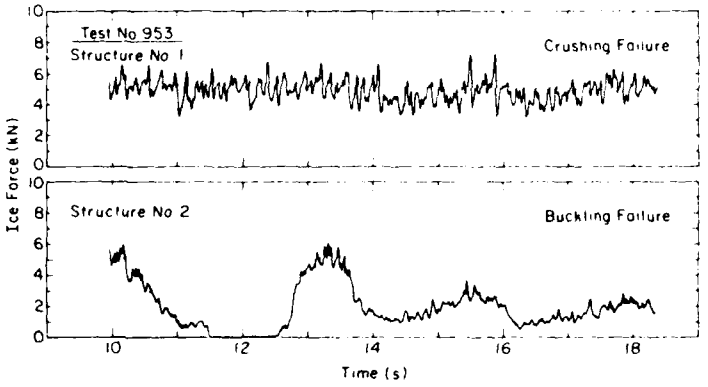

c. Test 953, crushing at one structure and buckling at the other.

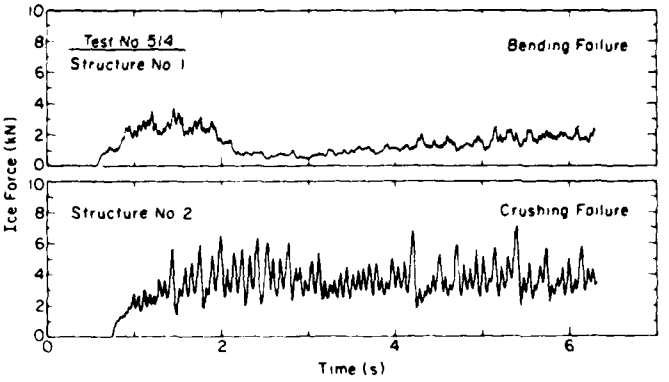

d. Test 514, crushing at one structure and bending at the other.

Figure 6. Ice force records.

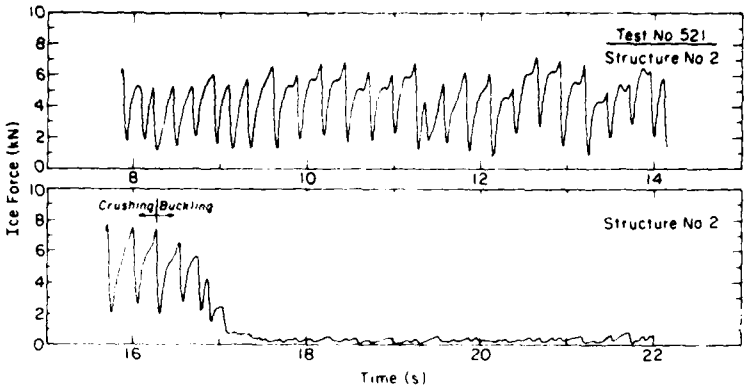

e. Test 521, transition from crushing to buckling.

Figure 6 (cont'd). Ice force records.

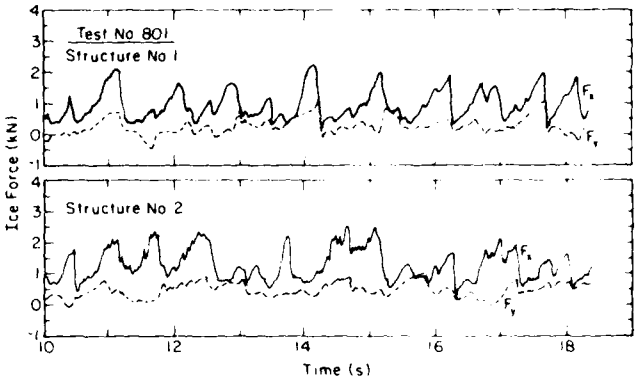

a. Test 801; d = *64 mm*, S = *259 mm.*

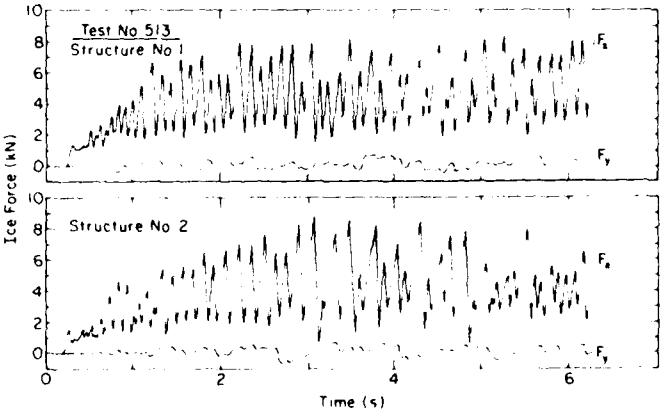

b. Test 513; d = *152 mm*, S = *1008 mm.*

Figure 7. Typical longitudinal and transverse ice force records.

Lee (1981) and Sodhi (1983) have shown that a higher rate of loading requires a higher load for the ice sheet to buckle. Thus a crushing failure can result at higher ice velocities because less force may be required for a crushing failure than that for a buckling failure.

Crushing failure

In this section we will discuss experimental results for continuous crushing failure. A summary of tests results is given in Table B2, which lists maximum longitudinal ice force (F_{xmax}), the mean longitudinal ice force (F_{xmean}) and the maximum ice force in the transverse direction (F_{ymax}) during each test. The mean force was computed over that period of time when continuous crushing took place. For instance, the mean force was computed for the entire duration of the force record shown in Figure 6a, whereas the forces were averaged between the time interval of 5 to 10.5 seconds of the force record shown in Figure 6b.

For a test series, we observed no dependence of ice forces on velocity for continuous crushing (Table B2). Michel and Toussaint (1977) compiled data on uniaxial compressive strength and indentation strength of ice and they also find no dependence of compressive strength on the strain rate when it is in the brittle range (i.e. $\epsilon > 10^{-2}\ s^{-1}$). They give an approximate expression for the strain rate (ϵ) in the ice around a structure as

$$\epsilon = (v/4\ d) \tag{1}$$

where v is the velocity and d the diameter of indentor (cylindrical structure in this case). Using eq 1, we found that the range of strain rate in our experiments was 0.02 s^{-1} to 0.1 s^{-1} for the 152-mm-diameter structures, 0.079 s^{-1} to 0.197 s^{-1} for the 64-mm-diameter structures and 0.021 s^{-1} to 0.082 s^{-1} for 305-mm-diameter structures. Although the strength and strain rate relationship for urea-doped ice has not been established, the high strain rates in our experiments can be assumed to be in the brittle failure zone, in which the crushing loads are independent of strain rate. Frederking et al. (1982) have reported an increase of ice forces with velocity, but the scatter in their data does not suggest any trend for the range of velocities and diameters used in our tests. Since the ice forces are not dependent upon the velocity, the ice forces discussed in later sections are the average ice force for a test series.

In the following sections we discuss the ice crushing forces and take into account the aspect ratio effect, the interaction effects of two structures and the dominant frequency in the ice force records.

Aspect ratio effect. Since the test series were performed with different ice thicknesses and strengths, it is only meaningful to compare force data obtained from different tests by taking the effect of the aspect ratio (structure diameter/ice thickness) into account using the following equation:

$$F_{xmax} = f(d/h)\sigma_c dh \tag{2}$$

where σ_c is the uniaxial confined compressive strength of columnar ice, d the diameter of the structure and h the ice thickness; $f(d/h)$ is a function expressing the effect of aspect ratio (d/h).

When the distance between the two structures was small, the measured forces might have been affected by the interaction between structures. Therefore, the following discussion is limited to the tests when the distance between the structures was more than five times the diameter (see *Interaction Effects on Ice Forces* section for discussion of how this criterion was obtained). The average and range of F_{xmax} and F_{xmean} are plotted with respect to the aspect ratio d/h in Figure 8. To quantify the effect of aspect ratio, we chose the following equation proposed by Afanas'yev et al. (1972):

$$F_{xmax} = \sqrt{5(h/d)+1}\ \sigma_c dh. \tag{3}$$

In this study we assume the confined compressive strength (σ_c) to be a multiple of unconfined compressive strength (σ_u), i.e., $\sigma_c = A\sigma_u$, where A is a constant.

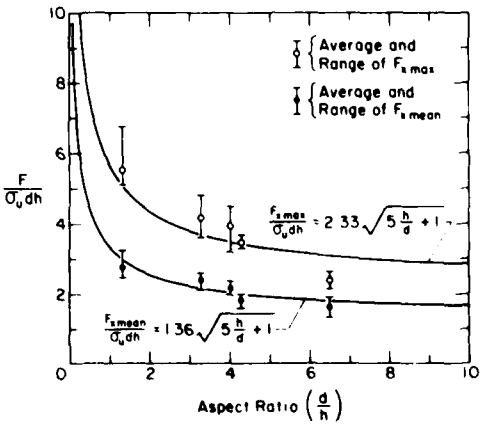

Figure 8. Ice forces versus aspect ratio (d/h).

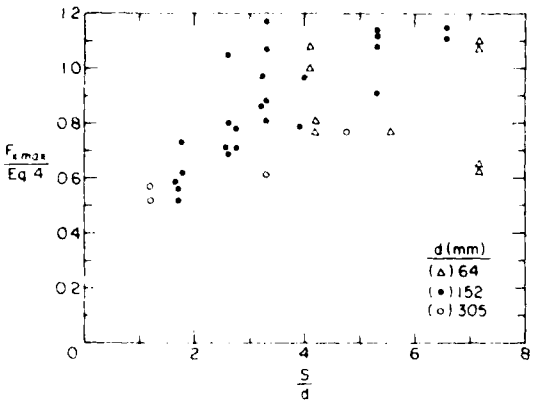

Figure 9. Normalized maximum forces versus ratio of center-to-center distance to structure diameter (S/d).

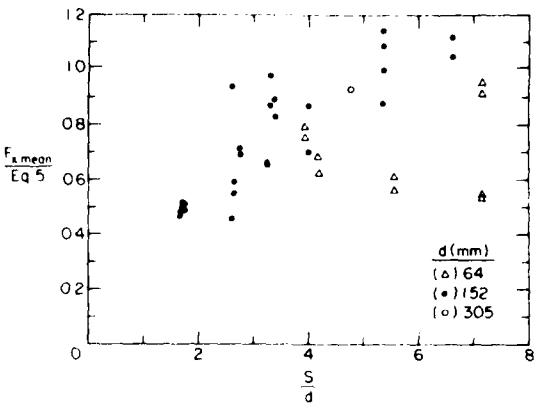

Figure 10. Normalized mean forces versus ratio of center-to-center distance to structure diameter (S/d).

A nonlinear regression analysis was performed on the data for the maximum and mean force levels to determine the coefficient A. Although the number of data points are few (due to the five times diameter separation criterion), the aspect ratio effect can be expressed by the following equation for the maximum force level:

$$F_{xmax} = 2.33 \sqrt{5(h/d)+1}\ \sigma_u dh. \qquad (4)$$

Similarly, the mean force F_{xmean} is given by

$$F_{xmean} = 1.36\sqrt{5(h/d)+1}\ \sigma_u dh. \qquad (5)$$

Plots of eq 4 and 5 are also shown in Figure 9.

Equations 4 and 5 will be used in the following discussion to represent the ice forces acting on isolated structures.

Interaction effects on ice forces. Any interaction between two structures that are situated side by side can affect the magnitude of ice forces and the ice-induced vibrations. In this section, the interaction effect on ice forces will be discussed.

The maximum forces measured in each test F_{xmax} are normalized by the right-hand side of eq 4 in order to compare the maximum forces obtained from different test conditions. The average F_{xmax} from each test series is plotted in Figure 9 with respect to the ratio of the center-to-center distance S to the structure diameter d. When the structures are located far apart, the plots of normalized F_{xmax} are scattered around 1.0 in Figure 9 because eq 4 gives the maximum force on an isolated structure. The normalized F_{xmax} is definitely less than 1.0 as the distance between the structures decreases.

The same procedure is applied to the mean force levels F_{xmean} which are normalized with the right-hand side of eq 5. The normalized F_{xmean} is plotted with respect to S/d in Figure 10. The trend in Figure 9 is seen in Figure 10 also. The normalized forces approach a value of 0.5 also when the structures are very close to each other.

From the data shown in Figures 9 and 10 we can conclude that the ice action on two structures has no interference effects when the distance between their centers is greater than five times the diameter of the structure. This is in agreement with the results of Saeki et al. (1978) who conducted similar experiments with three cylindrical structures. On the basis of the data presented in Figures 9 and 10, an empirical formula may be established that accounts for the interaction effects between the two structures.

Several investigators (Frederking 1977, Ralston 1978, Reinicke and Remer 1978) have reported that the confinement of ice is important to the strength of columnar ice because it is dependent on hydrostatic stress. Although a criterion that fully describes the state of stress at failure has not been well established, it is recognized that the failure of ice depends on the hydrostatic stress developed due to confinement. We observed that the ice between the structures either cracked laterally or was completely pulverized. The ice between the structure failed without offering much resistance to them because the ice was not confined. Perhaps, transverse vibrations of the structures play a role in the failure of ice between the structures.

Average ratios of F_{ymax} to F_{xmax} over a test series are plotted in Figure 11 with respect to S/d. It can be seen that the ratio decreases with the in-

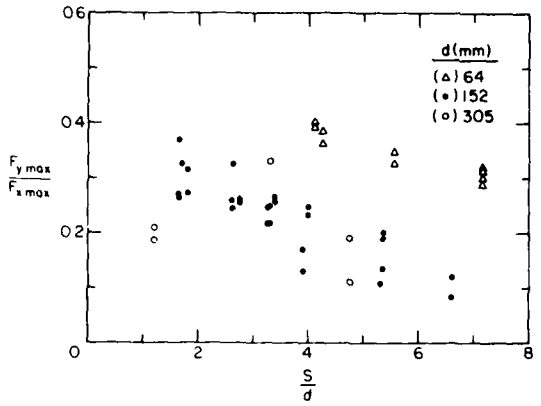

Figure 11. Ratio of maximum transverse and longitudinal forces (F_{ymax}/F_{xmax}) versus ratio of center-to-center distance to structure diameter (S/d).

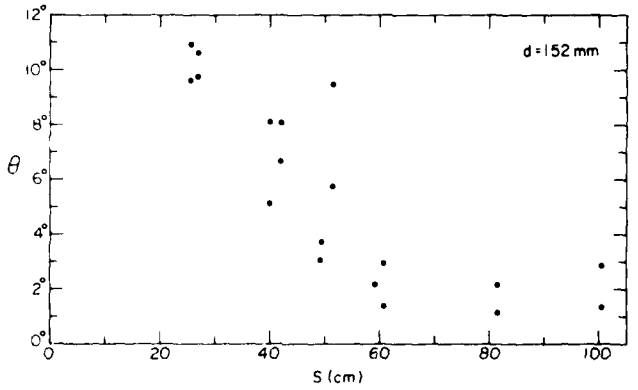

Figure 12. Resultant force direction θ versus S for the 152-mm-diameter structure.

crease in distance between the structures. For the 152-mm-diameter structures the ratio decreases from about 0.4 to 0.1. The same trend can be seen for the 64-mm-diameter structures, but the values of F_{ymax}/F_{xmax} are higher than those for 152-mm-diameter structures. For the 305-mm-diameter structures, it is difficult to see any trend due to the small number of data points, but the scatter in the data is in the same range as that for the 152-mm-diameter structures. This suggests that the data points for 305-cm-diameter structures might have the same behavior as that for 152-mm-diameter structures.

It should be noted that F_{xmax} and F_{ymax} did not occur at the same time. The angles of inclination of the resultant force, $\theta = \tan^{-1}(F_y/F_x)$ (see Fig. 1), were calculated over some intervals of time; the average values of θ are listed in Table B3. Figure 12 shows the variation of the average angle θ with respect to center-to-center distance for the 152-mm-diameter structures. This figure also shows that the angle decreases with the increase in S, and it is constant when the ratio S/d is more than 4.

The average value of θ may be considered to correspond to the location of the ice failure zone around a structure. When the structures are placed far apart, the ice tends to fail symmetrically around the structure, whereas when the structures are placed near each other the ice tends to fail on one side. We attribute this inclination of the resultant force direction to the reduced strength of ice between the structures.

It is interesting to note the variations of longitudinal and transverse forces for isolated structures, i.e., when $S/d \geq 4$. For the 64-mm-dia-

meter structures, both the ratios of F_{ymax}/F_{xmax} and the average angle of force direction are higher than those for the 152-mm-diameter structures. In Figure 7a the force-time histories of F_x and F_y for the 64-mm-diameter structures are shown. The lateral force F_y seems to be correlated with the longitudinal force F_x, and its magnitude is substantial in comparison to the longitudinal force. Similar force-time histories are shown in Figure 7b for the 152-mm-diameter structures. In this case, the lateral force F_y does not have any correlation with F_x, and its magnitude is very small in comparison to the magnitude of F_x. These observations may be explained in the following manner.

Relative to the structure diameter, the average size of broken pieces of ice for the 64-mm-diameter structures was larger than that for the 152-mm-diameter structures. If the concept of multiple failure zones, as proposed by Kry (1978, 1981), can be applied to the crushing failure around the two different structure sizes in our experiments, we may conclude that failure zones around the 152-mm-diameter structures were more in number than around the 64-mm-diameter structures. Thus the resultant force generated by many failure zones around a large structure tends to be aligned along the direction of ice movement. Perhaps the mode of crushing action may be different for the two sizes, i.e., the 64-mm-diameter structure induced an indentation failure in the ice sheet, whereas the 152-mm-diameter structure induced a flaking type of ice failure. This point will be discussed further in relation to the dominant frequency in the ice force record.

Ice-induced vibration. In continuous crushing failure, the forces fluctuated considerably as shown in Figures 6a, 6c-e and 7. These fluctuations may have correlation with the frequency of ice failure during the ice-structure interaction; we will call the frequency of ice failure the frequency of ice-induced vibration. Since the natural frequency of the structures was much higher than the dominant frequencies in the ice force record, we believed there was no modification of ice forces in the measuring system due to structural vibration. For an isolated structure, it may be assumed that there is a correlation between the frequency of ice-induced vibration and the ice velocity (Neill 1976, Maattanen 1980). On the other hand, the interactions between two closely placed structures may alter that correlation because the forces generated between the structure and the ice sheet are affected.

We did Fourier transforms on the ice force records to obtain the dominant frequency of ice-induced vibration. The typical autospectra of force records are shown in Figure 13. The dominant frequency of ice-induced vibration can be clearly established from autospectra, and these are listed in Table B4 and plotted in Figure 14 with respect to the ice velocity. For the structures placed far apart, Figures 14c-e show a trend of increase in the dominant frequency of ice-induced vibration with increase in ice velocity. On the other hand, there is no such trend in Figures 14a and b for the closely placed structures. Moreover, the autospectra for the isolated structures have a distinct peak (Fig. 13a), whereas it becomes difficult to pick a distinct peak in the autospectra for the structures placed close to each other (Fig. 13b). These two phenomena—the lack of correlation between the dominant frequency and velocity, and the complicated power spectra—may be

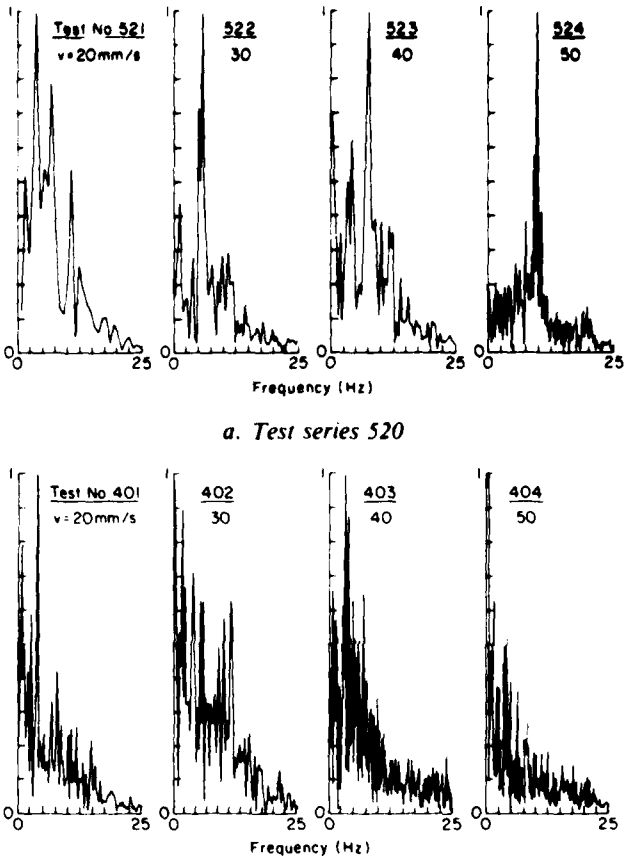

a. Test series 520

b. Test series 400

Figure 13. Autospectra of ice force records. The ordinate values have been normalized by the maximum value in the autospectra.

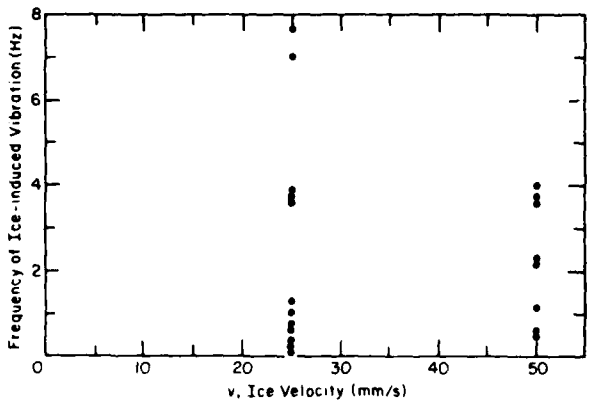

a. Test series 110 to 140, d = *152 mm.*

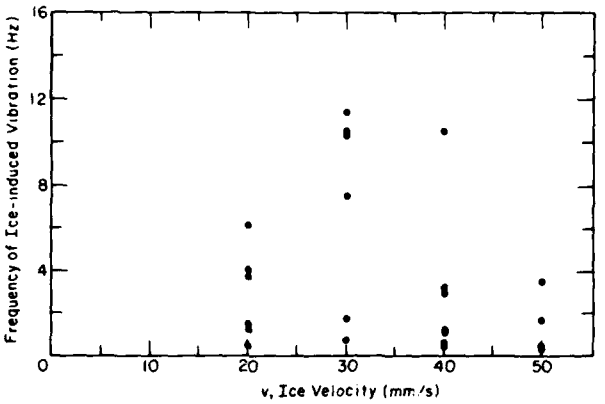

b. Test series 400 to 430, d = *152 mm.*

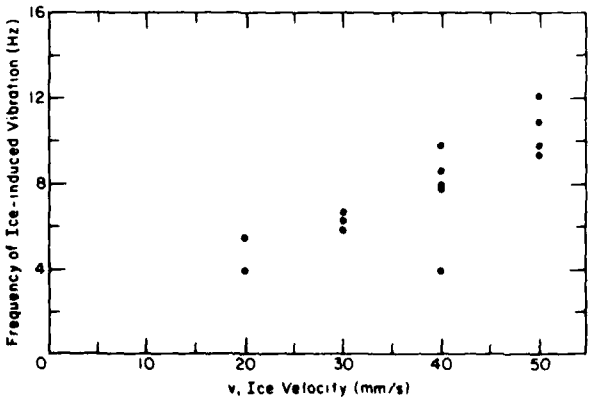

c. Test series 500 to 520, d = *152 mm.*

Figure 14. Ice-induced vibration frequency versus velocity.

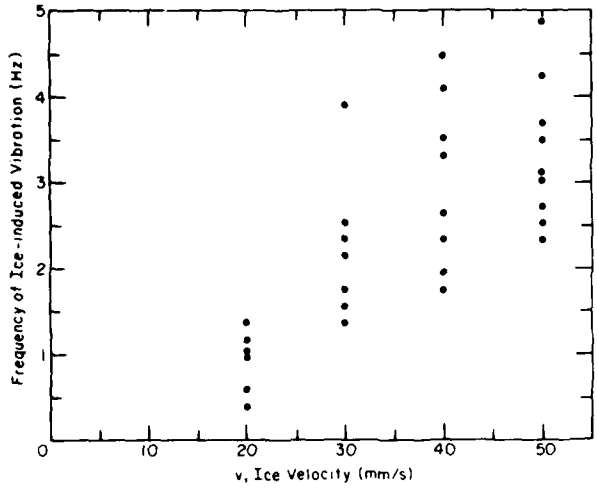

d. Test series 800 to 860, d = *64 mm.*

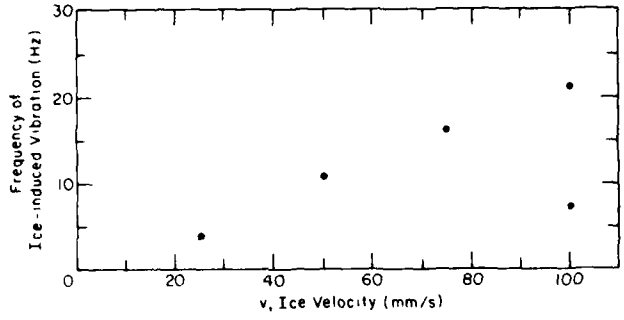

e. Test series 960, d = *305 mm,* S = *1450 mm.*

Figure 14 (cont'd). Ice-induced vibration frequency versus velocity.

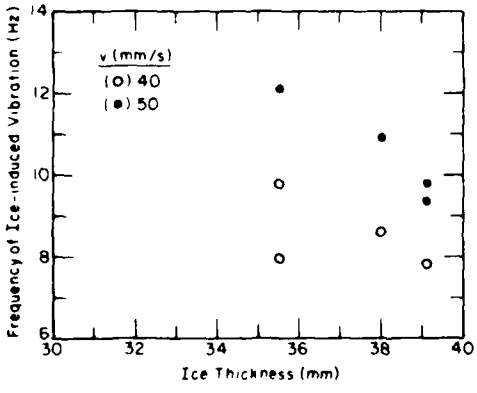

a. Test series 500, 64-mm-diameter structure.

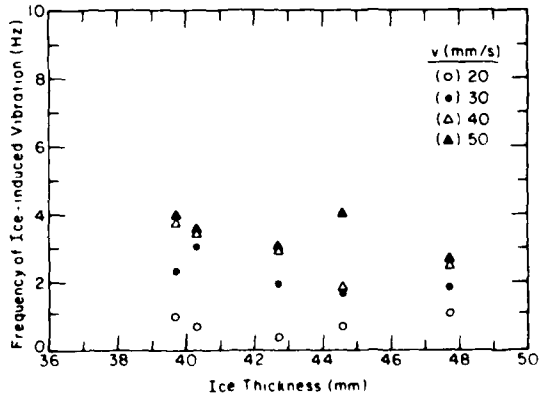

b. Test series 800, 152-mm-diameter structure.

Figure 15. Ice-induced vibration frequencies versus ice thickness.

considered an effect of interaction between two structures. We also observed that the interaction effects did not exist in the test series where the distance between the structures was more than five times the diameter.

Since a relationship exists between the frequency of ice-induced vibration and velocity for the tests on isolated structures, a discussion on this relationship is presented below.

Neill (1976) had a simple explanation. He said that the ice tends to break into fragments of a certain size distribution and that this size distribution together with velocity determines a frequency spectrum. Thus it is reasonable to assume that the frequency of ice-induced vibration may be related to the size of the ice failure zones in front of the structure and directly proportional to the ice velocity. Further, the size of ice failure zones may be dependent on ice thickness. To explore such dependence, the frequencies of ice-induced vibrations are plotted with respect to the ice thickness for the tests on 64-mm-diameter structures in Figure 15a and for the tests on 152-mm-diameter structures in Figure 15b. In Figure 15a, the averages of frequency obtained from two structures are plotted. In spite of the limited data, a trend of decreasing frequency with increasing ice thickness is tenable.

Maattanen (1980) proposed the following equation that estimates an upper bound for the frequency of the ice-induced vibration

$$f = kv\,\sigma_c\,hd \tag{6}$$

where f is the frequency, k is the stiffness of the structure, σ_c is the compressive strength, h is the ice thickness, d is the diameter of the structure, and v is the ice velocity. As shown by experimental results, the frequency is proportional to ice velocity, and it may be proportional to the inverse of ice thickness. Although the effect of strength on the frequency cannot be explicitly determined, we assume it to be of secondary importance as the variations of ice strength in our experiments were small. If the frequency is to be proportional to the inverse of ice thickness, the changes in frequency should not be large because the range of ice thickness was 35 to 50 mm. If the frequency of ice-induced vibrations is to be proportional to the inverse of the structure diameter according to eq 6, the frequencies of ice-induced vibration for the tests on the 64-mm-diameter structures should show frequencies at least 2.4 times larger than the tests on 152-mm-diameter structures. But contrary

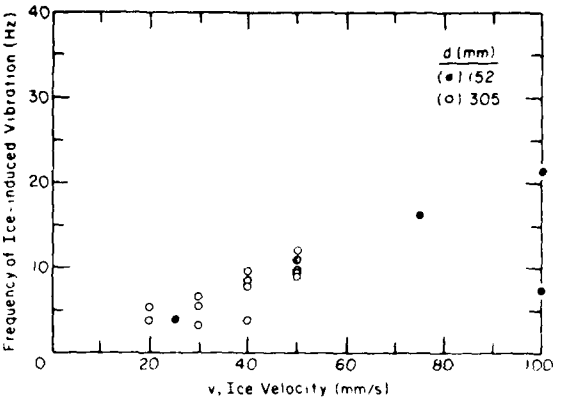

Figure 16. Combined plot of ice-induced vibration frequency versus velocity for test series 500 and 900.

results are shown in Figures 14c and d—the frequency of ice-induced vibrations for the tests on the 152-mm-diameter structures is much higher than that for 64-mm-diameter structures for the same velocities. However, Maattanen* maintains that eq 6 is derived from the theory of self-excited vibration of slender structures, and the structure in our experiment was much too rigid for the application of this theory.

The frequencies of ice-induced vibration for the tests on the 305-mm-diameter structures and the 152-mm-diameter structures are plotted with respect to velocity in Figure 16, and it is surprising to note that they are in the same range. To explain the above results, the frequency of ice-induced vibration may be assumed to be related to the size of ice failure zones, which in turn may depend upon the ice thickness, the structure diameter or the aspect ratio (d/h). A small diameter structure causes a large failure zone relative to its size, whereas the ice tends to fail in several places around a large structure (Kry 1978, 1981). It is well known that the mode of failure for small aspect ratios is an indentation type whereas the failure mode for large aspect ratios is a flaking type. As a result of different modes of ice crushing, we may expect different sizes of failure zones for different aspect ratios.

To test this hypothesis, the frequency of ice-induced vibration is plotted with respect to v/h in Figure 17, and the lines of best fit through the data points suggest the following relation:

* Personal communication with M. Maattanen, 1982.

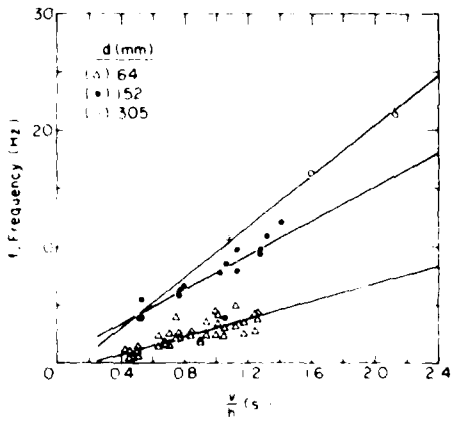

Figure 17. Ice-induced vibration frequencies versus ratio of relative velocity to thickness of ice sheet for different structure diameters.

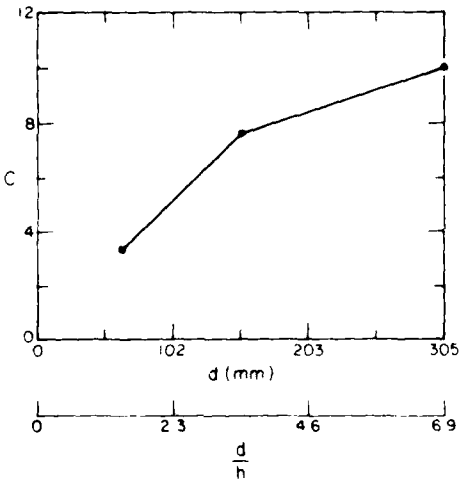

Figure 18. Coefficient C versus structure diameter (d) *and aspect ratio* (d/h).

$$f = C\,v/h \tag{7}$$

where C is a nondimensional coefficent dependent on the aspect ratio. The values of C are plotted with the respect to the structure diameter d and the aspect ratio in Figure 18 where h is the average ice thickness for all experiments. Although the experimental results are not extensive enough to test this hypothesis conclusively, we can see from the limiting value of C in Figure 18 that the frequency of ice-induced vibrations tends to be independent of the structure diameter or the aspect ratio.

Buckling failure

It is well known that the ice fails by buckling when the aspect ratio is high. In this experimental study the aspect ratio ranged from 1.33 to 7.27 and a few buckling failures were observed; these were two types: one when the ice sheet buckled around each structure separately, and the other when the ice sheet buckled simultaneously around both structures and had a common failure zone. The latter is an interaction effect. The types of buckling failure are listed in Table B5 along with the measured buckling loads.

Several theoretical studies on buckling of floating ice sheets have been conducted (Sodhi and Hamza 1977, Wang 1978, Sodhi 1979). Sodhi et al. (1982a) have reported that experimental buckling loads agree well with theoretical buckling loads.

Figure 19 shows the plots of normalized buckling load versus the ratio of diameter to characteristic length. All the data listed in Table B5 are plotted in Figure 19. Data points for the separate failures are scattered around the theoretical buckling load for frictionless boundary conditions at the ice-structure interface. A frictionless boundary condition implies no restraint to rotation or vertical displacement of the ice edge, whereas a hinged boundary condition implies complete restraint to vertical displacement and no restraint to rotation of the ice sheet at its edge. The experimental data for simultaneous buckling failure are generally less than those for separate buckling failure. Since the smooth surface of the structures simulated a frictionless boundary condition, we can conclude that the experimental buckling load agrees with the theoretical buckling load for the ice sheet buckling around each structure separately.

There is no theoretical analysis available for the buckling of an ice sheet against two structures simultaneously. If we consider two closely placed structures to be a single structure because of one failure zone in the ice sheet, the buckling load can be summed, and the effective width of the two structures B_e will be the sum of the center-to-center distance S plus the diameter of each structure d. The combined results are listed in Table B6 and are plotted in Figure 20. The number of data points is too small to make any definitive statements, but most of the data fall slightly below the theoretical buckling load for frictionless boundary conditions. Since the surface of the structures were smooth and nearly frictionless, we consider this modification of estimating the buckling load on two structures to be adequate.

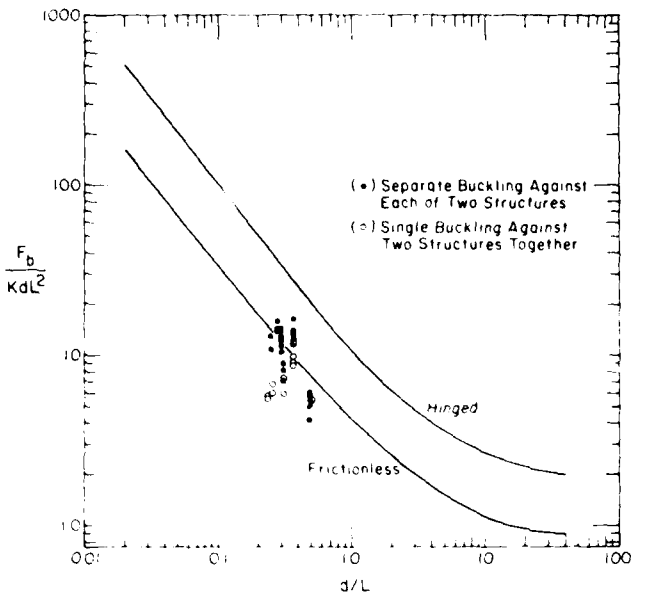

Figure 19. Normalized buckling loads F_b/KdL^2 versus ratio of structure diameter to characteristic length of ice sheet (d/L).

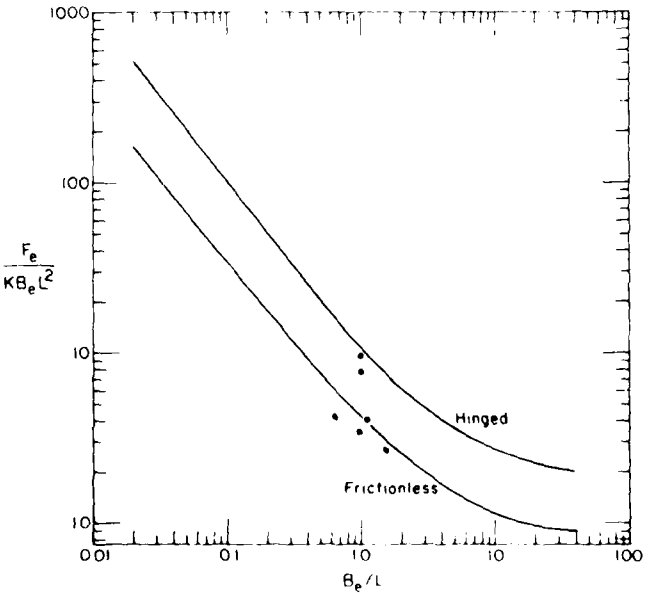

Figure 20. Normalized buckling load F_e/KB_eL^2 against two structures versus ratio of equivalent width of two structures to characteristic length (B_e/L).

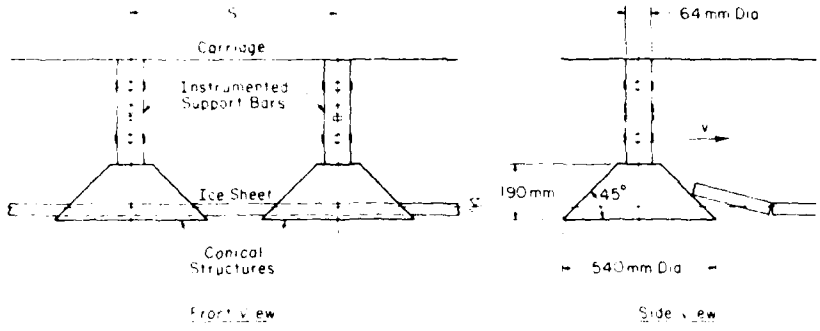

Figure 21. Experimental setup for conical structures.

Conical structures

We conducted experiments similar to those described earlier on two conical structures that were placed close to each other. A schematic of the conical structures is shown in Figure 21. A description of how these structures were fabricated has been given earlier. In the following, the modes of ice failure and associated forces are discussed.

General observations

Basically, we observed two failure modes during ice action on the conical structures. Either the ice sheet failed around each structure separately (Fig. 22a) or it failed around both structures simultaneously, having a common area of failure (Fig. 22b). Generally, the separate failure zones became more pronounced as the distance between two structures increased. Even if a common failure zone was produced initially, successive failure zones could be separate, as depicted in Figure 22a.

Ice action against an isolated conical structure resulted in bending failure of the ice sheet, with radial and circumferential cracks. The size of the affected area of the ice sheet is related to its strength and elastic properties. With ice action against two conical structures, the occurrence of a common zone of failure (Fig. 22b) is dependent on the ability of the ice to support itself across the span between the structures. As the distance increases, the ice sheet between the structures is not lifted because of its weight and limited strength. When the structures are far apart, they act as isolated structures.

Ice forces on conical structures

Typical portions of records of measured ice forces are shown in Figure 23 for the failure of an ice sheet against two conical structures. The maximum force F_{max} and the initial peak force F_i for each test are summarized in Table B7 along with the experimental conditions.

Since the experiments were made on different ice sheets, a direct comparison of results of different tests is meaningless. To compare data obtained from various tests, we chose the formulation proposed by Ralston (1977) for normalization. For calculating the theoretical ice force F_r from Ralston's formulation, the coefficent of friction is assumed to be 0.05 for the structures with the aluminum surfaces and 0.15 for the structures with the plastic surfaces.

Normalized forces, i.e., measured forces divided by the theoretical force F_r, are summarized in Table B8. Normalized forces F_{max} and F_i are plotted with respect to ice velocity in Figures 24 and 25 respectively. In Figure 24, the trend is obvious, whereas it is not as pronounced in Figure 25. In spite of considerable variation in the data, there is a tendency for the forces to increase with velocity.

Although it is not the purpose of this study to evaluate Ralston's formulation, the predicted theoretical forces are always larger than the experimental forces except in a few cases. Ralston himself stated that this theory would overestimate an ice force as much as 30% due to an overestimation of contact area around the waterline. We have found this to be the case for maximum ice forces at low ice velocities (Fig. 24 and 25). But, the effect of ice velocity mentioned earlier is not taken into account in Ralston's formulation. We found that the normalized initial force (F_i/F_r) was less than the normalized maximum force (F_{max}/F_r) (see Fig. 24 and 25). We attribute this to the configuration of the ice sheet being prepared to have a straight edge for initial contact; the failure took place before the structure could make extensive contact with the ice sheet. Moreover, we

a. Separate failure zone around each structure.

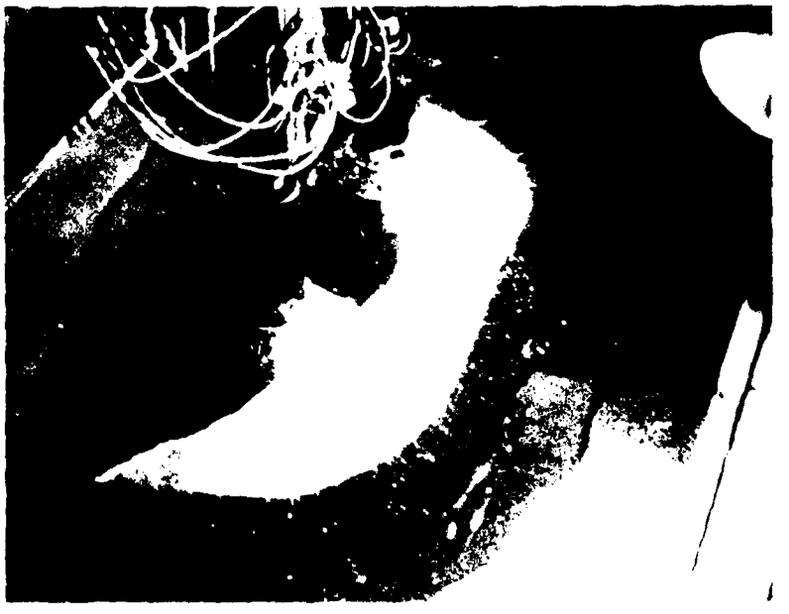

b. Failure zone common for both structures.

Figure 22. Failure of an ice sheet against two conical structures.

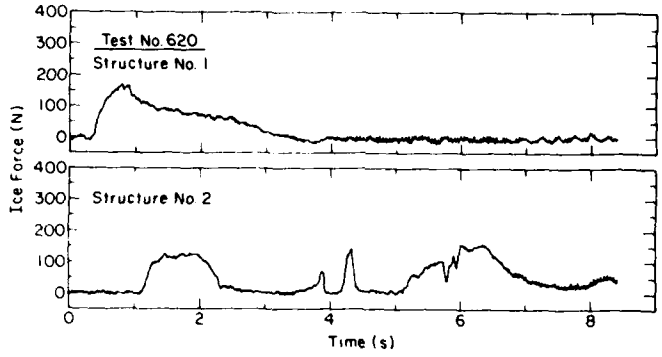

a. Separate failure zone around each structure.

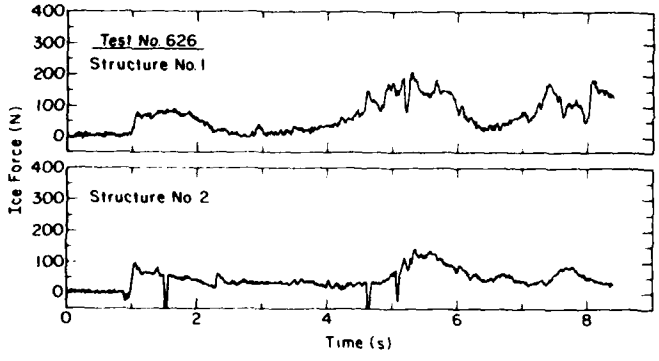

b. Failure zone common for both structures.

Figure 23. Ice force records for failure of ice against two conical structures.

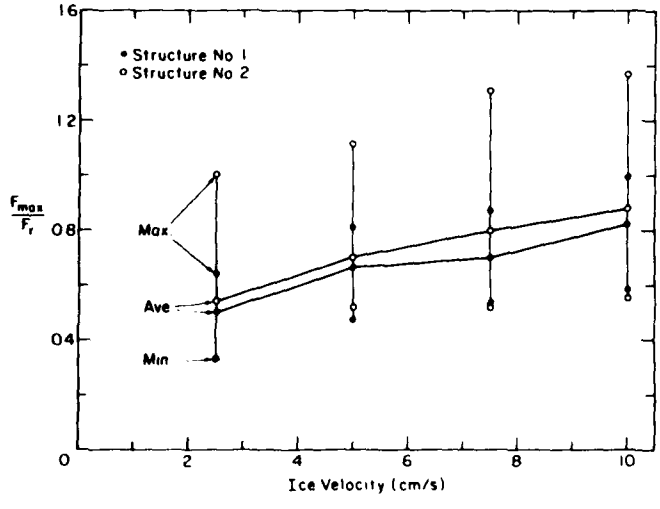

Figure 24. Normalized maximum ice force (F_{max}/F_r) versus ice velocity.

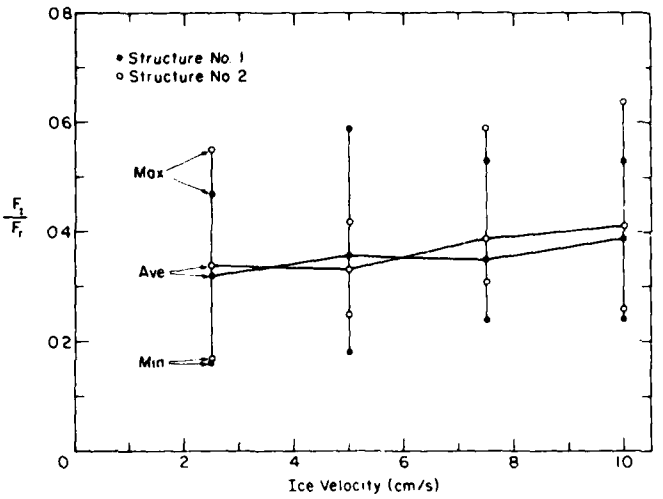

Figure 25. Normalized initial peak force (F_i/F_r) versus ice velocity.

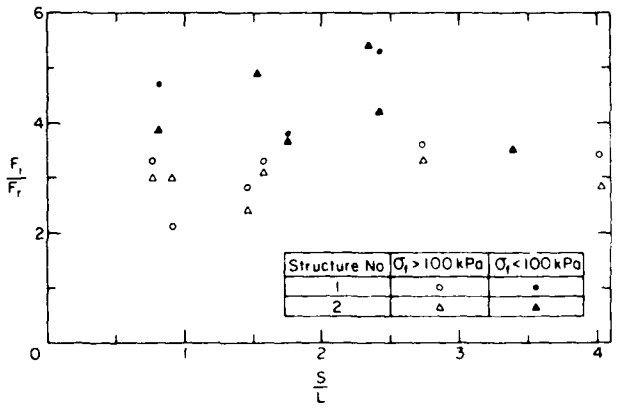

Figure 26. Ratio of initial peak ice force to theoretical ice force (F_i/F_r) versus ratio of center-to-center distance between structures to characteristic length (S/L).

sometimes observed the broken ice blocks sliding down into the water instead of climbing up the structure right after the first failure took place.

In Figure 26, the F_i/F_r ratios are plotted with respect to the S/L ratios (this is normalized center-to-center distance between structures relative to characteristic length of ice sheet) to investigate the influence of distance between the structures. On the basis of the scatter in Figure 26, there appears to be no influence of distance between the structures on the initial ice force F_i.

CONCLUSIONS

We conducted small-scale experiments by pushing pairs of cylindrical and conical structures through floating ice sheets to determine the interaction effects on the ice forces of the distance between the structures. The properties of the model ice sheet were measured intermittently during the experiments to enable presentation of results in nondimensional form.

For the tests with cylindrical structures, we

varied their diameter, the distance between them, and their relative speed with respect to the ice. The modes of ice failure were crushing, buckling and sometimes bending.

We found an aspect ratio effect in the maximum and mean ice forces when the structures were placed far apart. Velocity had no effect on the measured ice forces.

The maximum and mean values of the ice forces were affected when the distance between the structures was small. For distance between the structures greater than four to five times the structure diameter, the above influence was nonexistent. When the distance between the structures was large, the resultant force was almost wholly in the longitudinal direction. When the distances between the structures became smaller, the direction of resultant force shifted outward, indicating that the ice failure zone occurred on the outer sides of the two structures. A similar effect was found for the mean direction of resultant ice forces.

The dominant frequency of the ice force vibrations was also affected by the proximity of the structures. When the structures were far apart, the dominant frequency of ice-induced vibration was directly proportional to velocity and inversely proportional to ice thickness. The constant of proportionality was found to be a nonlinear function of aspect ratio. More research is required to confirm this conclusion.

For structures placed far apart, the measured buckling forces were in agreement with theoretical buckling loads. When a common zone of buckled ice sheet formed because of the proximity of two structures, we achieved the agreement of experimental and theoretical buckling loads by summing the individual loads on two structures and taking the width of the combined structures to be the sum of distance between their centers and their radii.

For the tests on conical structures, bending was the main mode of ice sheet failure. When the structures were placed close to each other, a common bending failure zone developed. We found the mean and maximum ice forces to increase slightly with increasing velocity. There appeared to be no influence of the distance between the structures on the ice forces.

LITERATURE CITED

Afanas'yev, V.P., Iu. V. Dolgopolov and Z.I. Shvayshteyn (1972) Ice pressure on separate supporting structures in the sea. Trudy Leningrad, Arkt. i Antarkt. Inst., vol. 300, pp. 61-80. USA Cold Regions Research and Engineering Laboratory, Draft Translation 346. ADA 741873.

Frederking, R. (1977) Plane-strain compressive strength of columnar-grained and granular-snow ice. *Journal of Glaciology,* **18**(80): 505-516.

Frederking, R., J. Schwarz, E. Wessels and L. Hoffmann (1982) Model investigations of ice forces on cylindrical structures. *Proceedings, International Conference on Marine Research, Ship Technology and Ocean Engineering (INTER MARITEC 82), Hamburg, Germany.* Institute for Ship and Marine Technology, Technical University of Berlin, pp. 341-349.

Haynes, F.D., D.S. Sodhi, K. Kato and K. Hirayama (1983) Ice forces on model bridge piers. USA Cold Regions Research and Engineering Laboratory, CRREL Report 83-19.

Hirayama, K. (1983) Properties of urea doped ice in the CRREL test basin. USA Cold Regions Research and Engineering Laboratory, CRREL Report 83-8.

Kato, K., D.S. Sodhi, F.D. Haynes and K. Hirayama (1982) Uniaxial in situ compressive strength of model ice: A theoretical and experimental study. USA Cold Regions Research and Engineering Laboratory, CRREL Internal Report 775.

Kry, P.R. (1978) A statistical prediction of effective ice crushing stresses on wide structures. *Proceedings, 4th International Association of Hydraulic Research Symposium on Ice Problems, 7-9 August, Lulea, Sweden.* University of Luela. pp. 33-47.

Kry, P.R. (1981) Scale effects in continuous crushing of ice. *Proceedings, 5th International Association of Hydraulic Research Symposium on Ice Problems, 27-31 July, Quebec, Canada.* Laval University, pp. 565-580.

Lee, L.H.N. (1981) Dynamic buckling of an inelastic column. *International Journal of Solids Structure,* **17**: 271-279.

Maattanen, M. (1980) Ice force on fixed, flexible structures. A state-of-the-art report by the Working Group on Ice Forces on Structures, IAHR. USA Cold Regions Research and Engineering Laboratory, Special Report 80-26. ADA 089 674

Michel, B. and N. Toussaint (1977) Mechanisms and theory of indentation of ice plates. *Journal of Glaciology,* **19**(81): 285-300.

Neill, C. (1976) Dynamic ice forces on piers and piles: An assessment of design guidelines in the light of recent research. *Canadian Journal of Civil Engineering,* **3**(2): 305-341.

Ralston, T.D. (1977) Ice force design consideration for conical offshore structures. *Proceedings,*

4th International Conference on Port and Ocean Engineering Under Arctic Conditions (POAC '77), 26-30 September, St. John's, Newfoundland. Memorial University of Newfoundland, pp. 741-752.

Ralston, T.D. (1978) An analysis of ice sheet indentation. *Proceedings, 4th International Association of Hydraulic Research Symposium on Ice Problems, 7-9 August, Lulea, Sweden.* University of Lulea, pp. 13-31.

Reinicke, K.M. and R. Remer (1978) A procedure for the determination of ice forces—illustrated for polycrystalline ice. *Proceedings, 4th International Association of Hydraulic Research Symposium on Ice Problems, 7-9 August, Lulea, Sweden.* University of Lulea, pp. 217-238.

Saeki, H., T. Ono, A. Ozaki and S. Abe (1978) Estimation of sea ice forces on pile structures. *Proceedings, 4th International Association of Hydraulic Research Symposium on Ice Problems, 7-9 August, Lulea, Sweden.* University of Lulea, pp. 465-478.

Sodhi, D.S. and H.E. Hamza (1977) Buckling analysis of semi-infinite ice sheet. *Proceedings, 4th International Conference on Port and Ocean Engineering under Arctic Conditions (POAC '77), 26-30 September, St. John's, Newfoundland.* Memorial University of Newfoundland, pp. 593-604.

Sodhi, D.S. (1979) Buckling analysis of wedge-shaped floating ice sheets. *Proceedings, 5th International Conference on Port and Ocean Engineering under Arctic Conditions (POAC '79), 13-17 August, Trondheim, Norway.* Norwegian Institute of Technology, pp. 797-810.

Sodhi, D.S., F.D. Haynes, K. Kato and K. Hirayama (1982a) Experimental determination of the buckling loads of floating ice sheets. *2nd Symposium on Applied Glaciology, Hanover, New Hampshire.* Proceedings to be published in Annals of Glaciology.

Sodhi, D.S., K. Kato, F.D. Haynes and K. Hirayama (1982b) Determining the characteristic length of model ice sheets. *Cold Regions Science and Technology*, **6**(2): 99-104.

Sodhi, D.S. (1983) Dynamic buckling of floating ice sheets. *Proceedings, 7th International Conference on Port and Ocean Engineering Under Arctic Conditions (POAC '83), 5-9 April, Helsinki, Finland.* Vol. II, pp. 822-833.

Wang, Y.S. (1978) Buckling analysis of a semi-infinite ice sheet moving against cylindrical structures. *Proceedings, 4th International Association of Hydraulic Research Symposium on Ice Problems, 7-9 August, Lulea, Sweden.* University of Lulea, pp. 117-133.

APPENDIX A: RELATIONSHIP BETWEEN FLEXURAL STRENGTH AND IN-SITU UNCONFINED COMPRESSIVE STRENGTH

In situ unconfined compressive strength tests were performed before most of the test series according to the procedure illustrated in Figure 3a and described in detail by Kato et al. (1982). In addition, tests were also conducted to determine the flexural strength and characteristic length of floating ice sheets for all test series. But, as mentioned above, in situ unconfined compressive strength was not measured for some test series. The purpose of this appendix is to establish a relationship between the flexural strength (σ_f) and the unconfined compressive strength (σ_u) of model ice from the available data. This relationship has been used in this study to estimate the unconfined compressive strength of model ice when such measurements were not made.

Basically, we determined the in situ unconfined compressive strength by loading a cantilever beam with a flat indentor (Fig. 3a) and then monitoring the total force. A typical force record is shown in Figure A1. The unconfined compressive strength is the peak force divided by the area of the beam.

The data are plotted in Figure A2 in terms of σ_u/σ_f versus σ_f. We used nonlinear regression to determine the best fit curve, which is shown in Figure A2 and given below.

$$\sigma_u/\sigma_f = 1.4722 + 4.981 \exp(-0.01159\ \sigma_f). \quad \text{(A1)}$$

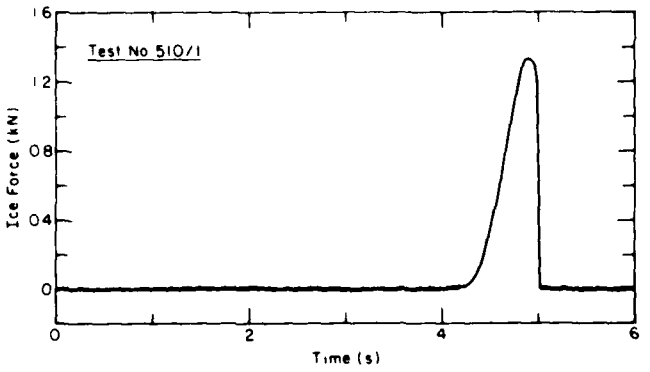

Figure A1. Typical ice force record during unconfined compressive strength test.

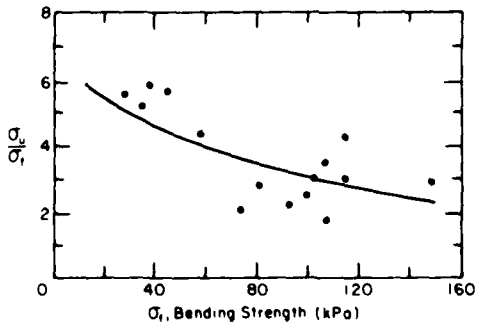

Figure A2. Ratio of unconfined compressive strength and flexural strength of ice (σ_u/σ_f) versus flexural strength.

APPENDIX B: TEST DATA

Table B1. Test conditions and observed failure modes (C = crushing, B = buckling, F = bending, C† = crushing with radial cracks).

Test series	*Test no.*	d *(mm)*	h *(mm)*	L *(mm)*	σ_f *(kPa)*	σ_u *(kPa)*	S *(mm)*	v *(mm/s)*	*Failure mode* *Structure 1*	*Structure 2*
110	110	152	47	740	141	292*	270	25	C	C
	111							25	C	C
	112							50	C	C
	113							50	C	C
120	120	152	48	720	91	290*	401	25	C	C
	121							25	C	C
	122							50	C	C
130	130	152	49	720	74	274*	493	25	C	C
	131							25	C	C
	132							50	C	C
140	140	152	49	720	57	244*	608	25	C	C
	141							25	C	C
	142							50	C	C
200	200	152	48	720	91	290*	253	25	C/F	C/F
	201							25	C	C
	202							50	C	C
210	210	152	50	740	42	202*	400	25	C	C
	211							50	C	C
220	220	152	50	730	37	200*	502	25	C	C
	221							25	C	C/F
	222							30	C	C
400	400	152	43	660	106	370	259	Uniaxial		
	401							20	C/B	C/B
	402							30	C	C
	403							40	C	C
	404							50	C	C
410	410	152	47	600	57	248	420	Uniaxial		
	411							20	C/B	C/B
	412							30	C/F	C/F
	413							40	C	C
	414							50	C	C
420	420	152	47	600	44	248	513	Uniaxial		
	421							20	C/F	C/F
	422							30	C	C/F
	423							40	C†	C†
	424							50	C†	C†
430	430	152	46	570	34	176	815	Uniaxial		
	431							20	C/F	C/F
	432							30	C	C/F
	433							40	C	C†
	424							50	C†	C†
500	500	152	35	520	148	432	815	Uniaxial		
	501							20	B	B
	502							30	B	B
	503							40	C	C
	504							50	B	C/B

Table B1 (cont'd). Test conditions and observed failure modes (C = crushing, B = buckling, F = bending, C† = crushing with radial cracks).

Test series	*Test no.*	d *(mm)*	h *(mm)*	L *(mm)*	σ_f *(kPa)*	σ_u *(kPa)*	S *(mm)*	v *(mm/s)*	*Failure mode*	
									Structure 1	*Structure 2*
510	510	152	38	550	114	342	1008	Uniaxial		
	511							20	B	C/B
	512							30	C/B	C
	513							40	C/F	C
	514							50	F	C
520	520	152	39	620	114	487	597	Uniaxial		
	521							20	C/B	C/B
	522							30	C/B	C/B
	523							40	C/F	C
	524							50	C	C
700	700	152	34	420	99	247	260	Uniaxial		
	701							20	B**	B
	702							30	B**	B
	703							40	B**	B/C
	704							50	B**	B/C
710	710	152	38	420	27	150	1012	Uniaxial		
	711							20	B**	B/C
	712							30	B**	B/F
	713							40	B**	B
	714							50	B**	B
720	720	152	40	500	37	215	604	Uniaxial		
	721							20	F	F
	722							30	F/B	F
	723							40	B	B
	724							50	F/B	C/B
800	800	64	40	590	107	186	259	Uniaxial		
	801							20	C	C
	802							30	C	C
	803							40	C	C
	804							50	C	C
810	810	64	45	590	80	224	352	Uniaxial		
	811							20	C	C
	812							30	C	C
	813							40	C	C
	814							50	C	C
820	820	64	48	540	73	149	454	Uniaxial		
	821							20	C	C
	822							30	C	C
	823							40	C	C
	824							50	C	C
850	850	64	40	540	102	307	454	Uniaxial		
	851							20	C	C
	852							30	C	C
	853							40	C	C
	854							50	C	C
860	860	64	43	540	92	204	267	Uniaxial		
	861							20	C	C
	862							30	C	C

Table B1 (cont'd). Test conditions and observed failure modes (C = crushing, B = buckling, F = bending, C† = crushing with radial cracks).

Test series	Test no.	d (mm)	h (mm)	L (mm)	σ_f (kPa)	σ_u (kPa)	S (mm)	v (mm/s)	Failure mode Structure 1	Failure mode Structure 2
								40	C	C
	863							50	C	C
	864									
								25	F	F
900	900	305	46	620	78	280*	367	50	F	F
	901							75	F	F
	902							100	F	F
	903									
								25	B/C	B/F
910	910	305	51	620	68	266*	1996	50	B	B
	911							75	C/F	C/F
	912							100	C	C
	913									
								25	F**	F
950	950	305	42	630	100	296*	1006	50	F**	B
	951							75	C/F**	B
	952							100	C/B	B
	953									
								25	C	B
960	960	305	47	630	75	276*	1450	50	C	B
	961							75	C	B/F
	962							100	C	C
	963									

* Estimated by eq A1.
** Force record not available.

Table B2. Measured ice forces from continuous crushing failure.

Test no.	d (mm)	S (mm)	v (mm/s)	Structure 1			Structure 2		
				F_{xmax} (kN)	F_{ymax} (kN)	F_{xmean} (kN)	F_{xmax} (kN)	F_{ymax} (kN)	F_{xmean} (kN)
110	152	270	25	6.98	1.71	2.93	6.07	1.88	2.91
111			25	6.95	2.00	2.72	5.72	1.74	2.61
112			50	6.96	1.96	2.04	5.44	1.94	2.43
113			50	5.86	1.58	2.67	5.65	1.65	2.53
120	152	401	25	7.67	1.24	2.98	6.10	1.54	2.68
121			25	6.74	1.70	3.01	5.70	2.21	2.63
122			50	5.04	1.60	2.33	4.90	1.64	2.41
130	152	493	25	6.38	1.59	2.77	7.30	1.20	2.89
131			25	8.67	2.09	2.89	6.38	1.19	2.98
132			50	6.14	1.51	2.53	5.15	1.57	2.47
140	152	608	25	6.59	1.23	3.69	7.39	1.60	3.73
141			25	7.49	1.66	3.64	6.82	1.42	2.77
142			50	4.95	1.65	2.56	4.95	1.21	2.50
200	152	253	25	4.87	1.17	2.34	4.95	1.31	2.14
201			25	4.72	1.17	2.17	4.70	0.92	2.33
202			50	4.53	1.45	2.18	4.38	1.48	2.01
210	152	400	25	5.00	1.55	3.28	3.66	0.13	1.68
211			50	6.59	1.37	3.15	4.17	0.37	1.46
220	152	502	25	6.32	1.12	3.08	5.52	1.14	3.42
221			25	6.89	1.63	3.34	5.85	0.81	3.11
222			50	4.64	1.25	2.50	5.15	1.57	3.48
401	152	259	20	5.49	1.02	2.70	4.40	1.02	2.31
402			30	4.91	1.87	2.93	5.22	1.41	2.75
403			40	4.05	1.71	2.34	3.89	1.56	2.52
404			50	5.34	1.66	2.68	4.97	1.60	2.41
411	152	420	20	5.00	1.32	2.14	4.49	1.04	2.57
412			30	5.67	1.13	3.67	4.85	0.97	2.92
413			40	4.57	1.29	2.14	4.67	1.29	2.46
414			50	6.69	1.30	2.88	4.51	1.41	2.47
421	152	513	20	6.02	1.21	3.84	6.33	0.89	3.88
422			30	6.26	1.47	3.63	5.88	1.14	3.58
423			40	5.84	1.68	3.81	5.74	1.85	3.00
424			50	4.17	1.44	2.35	4.97	1.84	2.26
431	152	815	20	4.68	0.60	3.09	4.41	0.51	2.64
432			30	5.57	0.82	3.08	4.96	0.51	2.79
433			40	5.70	1.55	3.24	5.77	1.61	3.06
434			50	4.93	1.28	2.79	5.03	1.30	3.24
503	152	815	40	8.60	0.82	4.64	8.32	0.74	3.72
504			50	—	—	—	7.75	1.15	4.47
511	152	1008	20	—	—	—	7.41	0.72	4.22
512			30	7.58	0.54	4.29	8.68	1.24	3.93
513			40	8.21	0.72	4.70	8.92	1.08	4.68
514			50	—	—	—	7.74	0.96	4.05

Table B2 (cont'd). Measured ice forces from continuous crushing failure.

Test no.	d (mm)	S (mm)	v (mm/s)	Structure 1			Structure 2		
				F_{xmax} (kN)	F_{ymax} (kN)	F_{xmean} (kN)	F_{xmax} (kN)	F_{ymax} (kN)	F_{xmean} (kN)
521	152	597	20	7.54	1.26	4.98	8.13	1.56	4.05
522			30	7.78	0.81	4.71	7.89	1.57	4.60
523			40	8.43	1.10	4.74	8.29	1.53	4.31
524			50	8.83	0.94	4.52	8.21	0.85	5.07
801	64	259	20	2.51	1.14	1.24	2.50	0.98	1.30
802			30	2.48	0.82	0.94	2.29	0.79	0.96
803			40	2.54	0.98	1.01	2.30	0.87	1.05
804			50	2.26	0.99	0.96	2.02	0.94	1.01
811	64	358	20	2.25	1.06	1.02	2.77	0.79	1.24
812			30	2.60	—	1.02	2.35	0.85	1.13
813			40	2.51	0.55	0.99	2.30	1.01	0.98
814			50	2.32	0.70	1.03	2.30	0.71	1.08
821	64	454	20	2.59	0.64	1.33	3.05	0.77	1.46
822			30	2.62	0.86	1.26	2.45	0.56	1.34
823			40	2.40	0.88	1.11	2.31	0.97	1.11
824			50	2.36	0.85	1.16	2.40	0.75	1.16
851	64	539	20	2.32	0.70	1.22	2.62	0.83	1.31
852			30	2.55	0.86	1.15	2.37	0.75	1.18
853			40	2.25	0.73	1.11	2.10	0.48	1.13
854			50	2.42	0.70	1.01	1.95	0.54	1.05
861	64	267	20	2.30	0.85	1.10	2.55	0.91	1.27
862			30	2.05	-0.84	0.97	2.50	0.87	1.08
863			40	1.95	0.81	0.91	1.90	0.67	0.98
864			50	2.00	0.70	0.91	1.80	0.63	0.95
912	305	1996	75	7.05	1.43	4.30	5.85	1.08	3.23
913			100	6.45	1.09	3.50	6.30	1.46	3.75
953	305	1006	100	7.20	2.37	4.81	—	—	—
960	305	1450	25	9.00	0.91	7.36	—	—	—
961			50	10.01	2.38	7.05	—	—	—
962			75	9.20	1.77	6.27	—	—	—
963			100	8.20	1.87	5.66	7.20	0.79	5.13

Table B3. Average angle of force direction.

Test series	S (mm)	Structure 1 θ (°)	Structure 2 θ (°)
110	270	10.60	9.75
120	401	5.14	8.08
130	493	3.09	3.77
140	608	2.97	1.32
400	259	10.90	9.65
410	420	8.08	6.67
420	513	9.48	5.76
430	815	3.03	1.49
500	815	2.18	1.15
510	1008	2.86	1.32
520	597	2.12	1.20
800	259	13.00	14.41
810	359	0.23	9.70
820	454	6.16	4.57
850	454	4.23	5.03
860	267	15.96	15.48

Table B4. Frequency of ice-induced vibrations.

Test no.	Dominant frequency (Hz) Structure 1	Dominant frequency (Hz) Structure 2	Velocity (mm/s)	Test no.	Dominant frequency (Hz) Structure 1	Dominant frequency (Hz) Structure 2	Velocity (mm/s)
110	0.13	0.78	25	511	—	5.47	20
111	1.04	3.64	25	512	6.64	6.64	30
112	3.78	1.17	50	513	8.59	3.91	40
113	4.04	2.34	50	514	—	10.94	50
120	0.26	0.39	25	521	3.91	3.91	20
121	7.68	3.91	25	522	6.25	5.86	30
122	0.65	0.65	50	523	7.81	7.81	40
130	1.30	3.78	25	524	9.38	9.78	50
131	0.65	0.39	25	801	0.98	0.39	20
132	3.65	3.78	50	802	3.91	2.15	30
140	7.03	0.26	25	803	4.49	2.34	40
141	3.90	3.77	25	804	2.73	4.26	50
142	2.21	0.52	50	811	0.99	0.39	20
401	1.56	0.52	20	812	1.76	1.56	30
402	0.78	1.77	30	813	1.95	1.75	40
403	3.00	3.26	40	814	4.89	3.13	50
404	1.69	0.39	50	821	1.04	1.17	20
411	1.56	—	20	822	1.37	2.35	30
412	10.42	—	30	823	2.34	2.64	40
413	1.30	0.65	40	824	3.05	2.34	50
414	0.52	0.39	50	851	1.37	0.59	20
421	4.04	1.30	20	852	2.54	2.15	30
422	11.45	10.55	30	853	3.32	4.10	40
423	10.55	0.52	40	854	4.26	3.71	50
424	3.51	3.51	50	861	0.39	0.39	20
431	3.75	6.15	20	862	2.54	1.37	30
432	7.50	—	30	863	3.52	2.34	40
433	1.30	1.17	40	864	2.54	3.51	50
434	0.52	0.52	50	960	3.91	—	25
503	9.77	7.95	40	961	10.89	—	50
504	—	12.10	50	962	16.34	—	75
—	—	—	—	963	7.39	21.41	100

Table B5. Buckling loads.

Test no.	S *(mm)*	L *(mm)*	d *(mm)*	v *(mm/s)*	F_b *(kN)*	F_b *(kN)*	*Type**
401	259	656	152	20	3.6	3.7	S
411	420	596	152	20	3.6	3.2	S
501	815	519	152	20	5.8	4.9	I
502	815	519	152	30	4.6	4.2	I
504	815	519	152	50	5.6	5.2	I
511	1008	550	152	20	6.3	6.5	I
512	1008	550	152	30	7.2		I
521	597	619	152	50	6.2	7.4	I
701	260	420	152	20	No data	2.3	S
702	260	420	152	30	No data	2.6	S
703	260	420	152	40	3.2	3.6	S
704	260	420	152	50	2.4	3.1	S
711	1012	415	152	20	3.5		I
712	1012	415	152	30	3.6	4.2	I
713	1012	415	152	40	3.1	3.4	I
714	1012	415	152	50	3.2	3.5	I
722	604	496	152	30	2.6		I
723	604	496	152	40	3.0	3.3	I
724	604	496	152	50	2.2	2.7	S
910	367	617	305	25	6.2	4.0	S
951	1006	630	305	50		5.0	I
952	1006	630	305	75		6.0	I
953	1006	630	305	100	6.0	6.0	I
960	1450	630	305	25		7.0	I
961	1450	630	305	50		6.5	I
962	1450	630	305	75		7.3	I

* I = buckling of ice sheet around each structure separately.
S = buckling of ice sheet around two structures simultaneously.

Table B6. Summed buckling loads when the two structures caused a single failure zone in the ice sheet.

Test no.	S *(mm)*	d *(mm)*	S + d *(mm)*	L *(mm)*	F_e *(kN)*
401	259	152	4114	656	7.3
411	420	152	5724	596	6.8
703	260	152	4124	420	6.8
704	260	152	4124	420	5.5
724	604	152	7564	496	4.9
910	367	305	6718	617	10.2

Table B7. Test conditions and ice forces on conical structures.

Test no.	h (mm)	σ_f (kPa)	L (mm)	S (mm)	v (mm/s)	Structure 1 F_{max} (N)	Structure 1 F_t (N)	Structure 2 F_{max} (N)	Structure 2 F_t (N)
600	27	115	384	560	20	75	60	75	50
601					50	120	45	65	40
602					80	125	65	110	30
603	29	105	415	1668	25	100	80	75	50
604					50	120	70	125	45
605					75	155	70	100	55
606					100	170	90	100	50
607	31	60	415	1008	25	75	75	70	50
608					50	130	95	110	50
609					75	140	85	105	55
610					100	150	85	120	55
611	37	117	723	555	25	185	85	185	100
612					50	280	155	175	100
613					75	325	110	275	105
614					100	400	180	300	85
615	41	103	636	998	25	235	120	170	110
616					50	280	160	180	110
617					75	290	120	180	110
618					100	400	180	235	100
619	43	102	545	1502	25	300	160	170	120
620					50	275	165	200	125
621					75	280	200	245	125
622					100	310	150	280	125
623	36	112	584	564	25	120	60	95	50
624					50	175	65	160	80
625					75	195	90	175	110
626					100	215	90	185	110
627	41	58	568	1000	25	140	110	70	70
628					50	190	85	135	70
629					75	200	90	150	75
630					100	240	95	215	80
631	41	72	441	1497	25	170	95	130	80
632					50	245	110	200	75
633					75	200	115	175	95
634					100	230	110	170	85
635	49	73	690	559	25	305	115	230	85
636					50	405	240	290	105
637					75	480	275	460	140
638					100	—	—	480	220
639	54	54	660	1005	25	—	—	320	175
640					50	—	—	210	135
641					75	—	—	360	105
642					100	—	—	385	205
643	55	63	645	1502	25	—	—	240	180
644					50	—	—	—	—
645					75	—	—	315	190
646					100	—	—	320	210

Table B8. Normalizied ice forces on conical structures.

Test no.	Structure 1		Structure 2		Test no.	Structure 1		Structure 2	
	F_{max}/F_r	F_i/F_r	F_{max}/F_r	F_i/F_r		F_{max}/F_r	F_i/F_r	F_{max}/F_r	F_i/F_r
600	0.36	0.29	0.46	0.31	623	0.33	0.16	0.45	0.17
601	0.58	0.22	0.40	0.22	624	0.47	0.18	0.53	0.27
602	0.61	0.32	0.68	0.19	625	0.53	0.24	0.65	0.38
603	0.44	0.35	0.42	0.28	626	0.58	0.24	0.74	0.38
604	0.52	0.31	0.69	0.25	627	0.55	0.43	0.33	0.35
605	0.68	0.31	0.55	0.31	628	0.75	0.34	0.55	0.35
606	0.75	0.39	0.55	0.28	629	0.79	0.36	0.60	0.38
607	0.46	0.47	0.56	0.40	630	0.95	0.38	0.63	0.40
608	0.81	0.59	0.88	0.40	631	0.55	0.31	0.25	0.33
609	0.87	0.53	0.84	0.44	632	0.82	0.35	0.68	0.31
610	0.93	0.53	0.96	0.44	633	0.64	0.37	0.75	0.39
611	0.46	0.21	0.57	0.31	634	0.74	0.35	1.08	0.35
612	0.69	0.38	0.54	0.31	635	0.69	0.26	0.53	0.24
613	0.80	0.27	0.84	0.32	636	0.92	0.54	0.82	0.30
614	0.99	0.45	0.92	0.26	637	1.08	0.62	0.72	0.40
615	0.54	0.28	0.49	0.32	638	—	—	0.70	0.62
616	0.65	0.37	0.52	0.32	639	—	—	1.00	0.55
617	0.67	0.28	0.52	0.32	640	—	—	0.66	0.42
618	0.92	0.42	0.67	0.29	641	—	—	1.13	0.33
619	0.64	0.34	0.45	0.32	642	—	—	1.20	0.64
620	0.59	0.35	0.53	0.33	643	—	—	0.64	0.48
621	0.60	0.43	0.65	0.33	645	—	—	0.84	0.59
622	0.66	0.32	0.74	0.33	646	—	—	0.86	0.56

A facsimile catalog card in Library of Congress MARC format is reproduced below.

Kato, K.
Ice action on pairs of cylindrical and conical structures / by K. Kato and D.S. Sodhi.
Hanover, N.H.: U.S. Army Cold Regions Research and Engineering Laboratory; Springfield, Va.: available from National Technical Information Service, 1983.
v, 42 p., illus.: 28 cm (CRREL Report 83-25.)
Prepared for Office of the Chief of Engineers by Corps of Engineers, U.S. Army Cold Regions Research and Engineering Laboratory under CWIS 31723.
Bibliography: p. 22.
1. Bridges. 2. Bridge piers. 3. Conical test structures. 4. Cylindrical test structures. 5. Ice. 6. Ice forces. 7. Interactions. 8. Interactions of two structures. 9. Pier spacing. I. Sodhi, D.S. II. United States. Army. Corps of Engineers. III. Cold Regions Research and Engineering Laboratory, Hanover, N.H. IV. Series: CRREL Report 83-25.

END

DATE
FILMED

1-83

DTIC